

# An assessment of representing land-ocean heterogeneity via convective adjustment timescale in the Community Atmospheric Model 6 (CAM6)

Bidyut Bikash Goswami<sup>1</sup>, Andrea Polesello<sup>1</sup>, and Caroline Muller<sup>2</sup>

<sup>1</sup>Institute of Science and Technology Austria

<sup>2</sup>ISTA

April 23, 2024

## Abstract

The time needed by deep convection to bring the atmosphere back to equilibrium is called convective adjustment timescale or simply adjustment timescale, typically denoted by  $\tau$ . In the Community Atmospheric Model (CAM), convective adjustment timescale is a tunable parameter with one value, 1 hour, worldwide. Albeit, there is no justified reason why one adjustment timescale value should work over land and ocean both. Continental and oceanic convection are different in terms of the vigor of updrafts and hence can have different longevities. So it is logical to investigate the prescription of two different convective adjustment timescales for land ( $\tau_l$ ) and ocean ( $\tau_o$ ). To understand the impact of representing land-ocean heterogeneity via  $\tau$ , we investigate CAM climate simulations for two different convective adjustment timescales for land and ocean in contrast to having one value globally.

Following a comparative analysis of 5-year-long climate simulations, we find  $\tau_l = 4$  hrs and  $\tau_o = 1$  hr to yield the best results. Particularly, we find better MJO simulations. Although these  $\tau$  values were chosen empirically and require further tuning, the conclusion of our finding remains the same, which is the recommendation to use two different  $\tau$  values for land and ocean.

1           **An assessment of representing land-ocean heterogeneity via**  
2           **convective adjustment timescale in the Community Atmospheric**  
3           **Model 6 (CAM6)**

4           **Bidyut Bikash Goswami<sup>1</sup>, Andrea Polesello<sup>1</sup>, Caroline Muller<sup>1</sup>**

5           <sup>1</sup>Institute of Science and Technology Austria (ISTA), Klosterneuburg, Austria

6           **Key Points:**

- 7           • Two distinct values of convective adjustment timescale,  $\tau$ , over land & ocean in the con-
- 8           convective parameterization scheme are prescribed.
- 9           • The mean climate stays qualitatively the same, except for a moister and colder near-surface
- 10          atmosphere for longer  $\tau$ s over the oceans.
- 11          • A primary gain of using two different  $\tau$ s for land and ocean is improved simulation of the
- 12          convectively coupled equatorial waves.

---

Corresponding author: B. B. Goswami, [bgoswami@ista.ac.at](mailto:bgoswami@ista.ac.at)

## Abstract

The time needed by deep convection to bring the atmosphere back to equilibrium is called convective adjustment timescale or simply adjustment timescale, typically denoted by  $\tau$ . In the Community Atmospheric Model (CAM), convective adjustment timescale is a tunable parameter with one value, 1 hour, worldwide. Albeit, there is no justified reason why one adjustment timescale value should work over land and ocean both. Continental and oceanic convection are different in terms of the vigor of updrafts and hence can have different longevities. So it is logical to investigate the prescription of two different convective adjustment timescales for land ( $\tau_L$ ) and ocean ( $\tau_O$ ). To understand the impact of representing land-ocean heterogeneity via  $\tau$ , we investigate CAM climate simulations for two different convective adjustment timescales for land and ocean in contrast to having one value globally.

Following a comparative analysis of 5-year-long climate simulations, we find  $\tau_O = 4$  hrs and  $\tau_L = 1$  hr to yield the best results. Particularly, we find better MJO simulations. Although these  $\tau$  values were chosen empirically and require further tuning, the conclusion of our finding remains the same, which is the recommendation to use two different  $\tau$  values for land and ocean.

## 1 Introduction

Deep convection is complex to parameterize [Arakawa, 2004]. While the explicit representation of deep convection is becoming a plausible option to navigate this "deadlock" [Randall *et al.*, 2003; Randall, 2013], for long-term projections of our climate, cumulus parameterization is still unavoidable. Hence, amidst the fierce emergence of convection-resolving models [Stevens *et al.*, 2019], various schemes to parameterize convection continue to develop. In particular, the recent decades have witnessed a surge of novel ideas that have accelerated this progress [Rio *et al.*, 2019, and references therein].

The "art" of tuning parameters used in convection parameterization schemes, or simply parameter tuning, plays a vital role in this development process [Hourdin *et al.*, 2017]. While deficiencies of convective parameterization are primary factors for model biases, it alone cannot alleviate all mode biases [Goswami *et al.*, 2017]. Hence, parameter sensitivity investigations are necessary not only to optimize the performance of a scheme but also to understand the extremities to which a scheme can be held responsible for biases in a simulation [Qian *et al.*, 2015; Goswami *et al.*, 2017]. In this study, we aim to contribute to understanding one tunable parameter, the convective adjustment timescale  $\tau$ , by investigating the sensitivity of climate simulations to two dif-

44 ferent  $\tau$  values for land and ocean in contrast to having one value globally in the Zhang-McFarlane  
45 convective parameterization scheme [Zhang and McFarlane, 1995, ZM95 hereafter] in the Com-  
46 munity Atmospheric Model (CAM), the atmospheric model of the Community Earth System Model  
47 [Danabasoglu et al., 2020].

48 In CAM, deep convection is represented using the Zhang-McFarlane (ZM) convection pa-  
49 rameterization scheme. The ZM is an adjustment-type convective parameterization scheme where  
50 the atmospheric instability is removed via an adjustment towards a background state. In ZM, con-  
51 vective available potential energy (CAPE) defines atmospheric instability, and  $\tau$  is the CAPE con-  
52 sumption time. In their paper, ZM95 used  $\tau$  values of 2, 4, and 6 hours. To quote ZM95, "The  
53 adjustment time scale determines the intensity and duration of convection for a given CAPE. With  
54 small  $\tau$  the convection is short-lived but intensity is high, on the other hand with larger  $\tau$  the con-  
55 vection is long-lived but of low intensity". ZM95 reported their scheme to be particularly sen-  
56 sitive to the choice of  $\tau$ . Since there is no strict range of  $\tau$ , several studies investigated the sen-  
57 sitivity of CAM simulations to different  $\tau$  values. For example, Mishra and Srinivasan [2010]  
58 used  $\tau=[1,\infty]$ . Contrasting water-vapor isotope simulations in a suite of CAM single-column sim-  
59 ulations with a range of  $\tau$  values, Lee et al. [2009] found their simulations to match better with  
60 satellite observations with  $\tau = 8$  hrs. Mishra [2011, 2012] prescribed  $\tau = 8$  hrs in global climate  
61 simulations and noted improvements in the simulations of tropical climate, especially the con-  
62 vectively coupled equatorial waves. Evaluating 22 tunable parameters in CAM, Qian et al. [2015]  
63 reported  $\tau$  as one of the most critical tuning parameters. In all of the above studies,  $\tau$  has a sin-  
64 gles value globally.

65 One value of  $\tau$  globally is not a logical choice because deep convection exhibits different  
66 behaviors over continents and oceans [Hagos et al., 2013; Matsui et al., 2016; Roca et al., 2017;  
67 Roca and Fiolleau, 2020]. Since the width of a thermal plume is steered by boundary layer height  
68 [Williams and Stanfill, 2002], a deep continental boundary layer generates wider updraft veloc-  
69 ities in deep convection [Lucas et al., 1994]. Matsui et al. [2016] provided a climatological view  
70 of the contrast between oceanic and continental convective precipitating clouds from long-term  
71 TRMM satellite multisensor statistics. They found large proportions of deep clouds over land.  
72 Zipser et al. [2006] also found the most intense storms typically over continents. These obser-  
73 vations suggest that the atmospheric deep convection over land is wider and stronger than those  
74 over the oceans. In other words, atmospheric convection over land is shorter lived than that over  
75 ocean [Roca et al., 2017]. It advocates for a shorter convection consumption time scale over land  
76 than over oceans which motivated us to address the following question: although two different

77  $\tau$  values incorporating land-ocean inhomogeneity are logical, is it fruit-bearing in a model-simulated  
78 climate? To answer this question, we investigate,

- 79 • response of the mean climate, and
- 80 • response of large-scale waves,

81 by contrasting 5-year-long climate simulations with and without incorporating land-ocean inho-  
82 mogeneity via  $\tau$  values.

83 Convective parameterization schemes, particularly adjustment-type schemes, are based on  
84 the idea that convection takes some time to stabilize the atmosphere to a background state. Es-  
85 sentially, this time taken is  $\tau$  in the ZM scheme. Although numerically  $\tau$  can have almost any value,  
86 it is decided based on a scale separation between the convective activity of the individual clouds  
87 and large-scale forcing. This concept is nicely depicted in Figure 1.1 of [Davies, 2008]. The graph  
88 in that figure is a function of timescales associated with convection, and consists of a turbulent  
89 initial segment indicating fluctuation of individual clouds, followed by a flat segment where these  
90 fluctuations smooth out, and finally a segment corresponding to longer time-scales that shows  
91 the evolution of the large scale forcing field itself. Conceptually, changing  $\tau$  within a reasonable  
92 range (within the flat segment of Figure 1.1 of [Davies, 2008]) should not result in a dramatic change  
93 in the mean state of the simulated climate. We shall investigate it in detail in the first part of our  
94 results section.

95 Some changes that we expect in our experiments are in the simulated organization of con-  
96 vection. The organization of convection comes from the dynamic and thermodynamic impacts  
97 of convection on the atmosphere. Simply put, it is the memory of convection [Davies *et al.*, 2009],  
98 i.e. the fact that convection changes the large-scale properties, and can make their environment  
99 favorable or unfavorable to subsequent convection. Identifying sources of convective memory  
100 in cloud-resolving simulations, Colin *et al.* [2019] argued that the persistence of the state of con-  
101 vection contributes to convective memory. Colin *et al.* [2019] also suggested that convective mem-  
102 ory and organization interact mutually. By altering  $\tau$  we essentially alter memory associated with  
103 convection. Hence, we expect to see changes in convective organization. Taking a cue from Mishra  
104 [2011], we anticipate improved convective organization in the tropics for longer  $\tau$ . However, land-  
105 ocean heterogeneity in  $\tau$  is a unique feature of our experiments that we argue is essential based  
106 on heterogeneity in the behavior of convection over land and ocean. As supporting evidence, we

107 shall present an analysis of equatorial waves focusing on the MJO to evaluate the organization  
 108 of convection in the second part of our results section.

109 The paper is organized as follows. A brief description of the methodology is provided in  
 110 Section 2. Section 3 evaluates the response of the model to different  $\tau$  values. Finally, a few con-  
 111 cluding remarks are provided in Section 4.

## 112 **2 Model and simulation details**

113 We used the atmospheric model of the Community Earth System Model, version 2.1.3 (CESM  
 114 2.1.3) [Danabasoglu *et al.*, 2020], that is the Community Atmosphere Model, version 6 (CAM6),  
 115 developed and maintained at the National Center for Atmospheric Research (NCAR), with lon-  
 116 gitude and latitude specifications  $1.25^\circ$  and  $0.9^\circ$ , respectively, and 32 vertical levels. We forced  
 117 the model by HadISST1 climatological monthly mean SST data provided by the Met Office Hadley  
 118 Centre [Rayner, 2003]. In short, we performed CESM “F2000climo” simulations. In general,  
 119 these are atmospheric simulations forced by present-day climatology. All simulations are 6 years  
 120 long, and we analyzed the last 5 years of each simulation since, for atmosphere-only simulations,  
 121 1-year spin-up is enough.

122 We performed 5 simulations. The one with out-of-the-box  $\tau$  value of 1 hour globally is called  
 123 the control (*CTRL*). In the next 3 simulations, we delayed the  $\tau$  value over ocean ( $\tau_O$ ) to 2, 3 and  
 124 4 hours keeping  $\tau$  over land ( $\tau_L$ ) 1 hour. We called these 3 simulations *EXPT<sub>2h</sub>*, *EXPT<sub>3h</sub>* and  
 125 *EXPT<sub>4h</sub>*, respectively. We performed a last 5<sup>th</sup> experiment, named *EXPT<sub>slow</sub>*, for which we used  
 126 a  $\tau$  value of 4 hours globally. Before starting our comparative analysis, we rename our first sim-  
 127 ulation as *EXPT<sub>fast</sub>*, which initially we had named CTRL, for clarity and better fluency of nar-  
 128 ration of our findings. Table 1 depicts the  $\tau$  values for different experiments.

129 Our analyses primarily show a comparison between the 5 aforementioned simulations. For  
 130 some analyses we have used outgoing long-wave radiation (OLR) from NOAA ( $2.5^\circ \times 2.5^\circ$ ; daily  
 131 from 01-Jun-1974 to 12-Dec-2019) [Liebmann and Smith, 1996] as observational benchmark.

## 133 **3 Results**

### 134 **3.1 Mean Climate**

135 Since about 75% of the global surface is ocean, in the simulations of the mean climate, we  
 136 expect a similar model response in our experiments by delaying  $\tau$  only over the oceans, as ear-

Experiment Name	$\tau_L$	$\tau_O$
<i>EXPT<sub>fast</sub></i>	1hr	1hr
<i>EXPT<sub>2h</sub></i>	1hr	2hr
<i>EXPT<sub>3h</sub></i>	1hr	3hr
<i>EXPT<sub>4h</sub></i>	1hr	4hr
<i>EXPT<sub>slow</sub></i>	4hr	4hr

**Table 1.**  $\tau$  values for different experiments

132

137 lier studies did by having a larger  $\tau$  globally. An evaluation of some of the mean features of sim-  
 138 ulated climate in our experiments confirm this. We find an increase in large-scale rainfall and a  
 139 decrease in convective rain going from *EXPT<sub>fast</sub>* to *EXPT<sub>slow</sub>* (Fig 1 and Supplementary Fig  
 140 S1). Similarly, we also notice warming in the lower levels, stronger warming in the upper lev-  
 141 els, slight cooling in the mid-levels; moistening in the lower levels, and drying in the mid-levels  
 142 (Fig 2 and Supplementary Fig S2). These features have been reported in earlier studies [for ex-  
 143 ample, Fig 8 in *Mishra and Srinivasan, 2010*].

144 Investigating the mean features for land and ocean separately, we notice in addition, lower  
 145 level (upper level) warming (cooling) is more (less) over land than over oceans (Fig 2). In the case  
 146 of moisture, the letter "S" patterned vertical structure over the ocean is more curvy and squeezed  
 147 down meaning lower level (middle level) moistening (drying) is stronger over oceans than over  
 148 land and the respective peaks are vertically closer to the sea surface. These profiles, all together,  
 149 indicate a model response to changes in  $\tau$  in terms of the distribution of atmospheric convection  
 150 and clouds, which impacts heating/cooling and moistening/drying of the air column (Supplemen-  
 151 tary Fig S2). Essentially these responses indicate an accumulation of convective instability in the  
 152 atmosphere with delaying of convective adjustment time scale. It is attributable to more low-level  
 153 warming over the continents and more low-level moistening over the oceans. More moistening  
 154 near the ocean surface is relatively straightforwardly understandable, and it is a consequence of  
 155 the atmosphere taking longer to convect with larger  $\tau$ . To a zero-order approximation, as a re-  
 156 sult of the near-surface moisture pile-up in the oceanic regions, there is a moisture deficit in the  
 157 lower levels over the continental regions (Fig 3 and Supplementary Fig S3a and S3b). Indeed it  
 158 is apparent, in relative sense, in Fig 3. Although  $q_O$  does not exhibit a clear moistening signal,

159 the land drying in  $q_L$  is profound. The consequences are reflected in terms of changes in cloud  
 160 cover. In an overall declining tendency of cloud cover, from  $EXPT_{fast}$  to  $EXPT_{slow}$ , over the  
 161 tropics high clouds decrease more steeply than low clouds. Low clouds decrease less rapidly over  
 162 the ocean compared to those over land (Fig 4). It should be noted that cloud categories are ob-  
 163 jectively defined in CESM. For example, low-level clouds are the ones below 700 hPa and high  
 164 clouds are between 400 and 50 hPa. Cloud covers are integrated for each model level correspond-  
 165 ing to respective cloud categories. In that regard, going from  $EXPT_{fast}$  to  $EXPT_{slow}$ , low-cloud  
 166 cover changes (Fig 4) are consistent with relative surface moistness over land and ocean (Fig 3).

167 Taken together, the altered vertical profiles of moisture and temperature, distribution of con-  
 168 vective and large-scale rainfall, and associated clouds are consistent with the idea that convec-  
 169 tion is short-lived and stronger for smaller  $\tau$  values and long-lived and weaker for longer  $\tau$  value.  
 170 It is also evident from the solution of the CAPE equation in the ZM scheme, which can be ex-  
 171 pressed as  $CAPE(t) = CAPE_o \exp(-\frac{t}{\tau})$  in the absence of large-scale CAPE generation, where  
 172  $CAPE_o$  is the values of CAPE at  $t = 0$ . A larger  $\tau$  in this expression means a slower decay of  
 173 CAPE. The duration of convection is essentially linked with its persistence and hence "mem-  
 174 ory". We discuss its impact on the simulation of the equatorial waves in the following section.

### 175 3.2 Simulation of MJO variance and propagation

176 Organization is a primary feature of tropical convection. It essentially means a cluster of  
 177 deep precipitating clouds tied together. An important question is, what brings these clouds to-  
 178 gether? In other words, what causes convection to organize? One idea to see the organization of  
 179 convection is through superpositions of convectively coupled equatorial waves (CCEWs). These  
 180 atmospheric waves and tropical convection are entangled. In the tropics, the atmosphere responds  
 181 to convective heating in terms of waves that, in turn, organize convection. Therefore, the fidelity  
 182 of a model in simulating tropical climate is essentially its ability to simulate the CCEWs. A stan-  
 183 dard metric to analyze CCEWs is the Takayabu-Wheeler-Kiladis (TWK) spectra [*Takayabu, 1994a,b;*  
 184 *Wheeler and Kiladis, 1999*]. Figure 5 depicts the symmetric and asymmetric TWK-spectra for  
 185 the observed and simulated outgoing long-wave radiation (OLR). Understandably, a striking fea-  
 186 ture of the TWK-spectra of observed OLR shown in Fig 5a and b is the spectral power near the  
 187 origin of the plots in the wavenumber range 1-5 and frequency 20-100 days, well known as the  
 188 MJO. The MJO is a combination of or envelope of other waves in the equatorial atmosphere. Hence,  
 189 the accuracy of MJO simulation is arguably a measure of the fidelity of accurate simulation of

190 waves in the atmosphere [Zhang *et al.*, 2020]. Guo *et al.* [2015] showed in detail that the accu-  
 191 racy of CCEW simulation is critical for a realistic MJO simulation.

192 A comprehensive review of the science of MJO is available in Zhang *et al.* [2020]. Promi-  
 193 nent observed features of MJO suggest that they are most active in the Indo-Pacific warm pool  
 194 with an eastward propagation. An interesting fact, along its path from the Indian to the Pacific  
 195 Ocean, is that an MJO passes over the Indonesian maritime continent (IMC). During this pas-  
 196 sage, MJO and the prominent diurnal variabilities in the meteorology over the IMC islands in-  
 197 teract and mutually influence each other. So much so that nearly half of the MJOs fail to prop-  
 198 agate into the Pacific. It is critical, therefore, to represent the land-ocean heterogeneity as real-  
 199 istically as possible in climate models. Hence, we expect our experiments with logically defined  
 200 different values of  $\tau$  for land and ocean to improve simulated MJO features. Here, we shall present  
 201 analyses evaluating the simulation of MJO variance and propagation. We can draw some idea  
 202 of MJO simulation in different experiments from Fig 5. In Fig 5, the foremost remarkable fea-  
 203 ture is the increase in spectral power in the MJO wave number and frequency range for experi-  
 204 ments with a longer  $\tau$ . A closer visual inspection reveals that the MJO spectral power does not  
 205 dramatically change from  $EXPT_{2h}$  to  $EXPT_{slow}$ . For other waves, no one simulation is remark-  
 206 ably better than the rest. Fig 5 loosely suggests that overall the symmetric signal waves are im-  
 207 proved for longer time scales, but there are no clear improvement for the antisymmetric part.

208 To bring out the active region of MJO we applied space-time filtering on OLR data con-  
 209 taining the signal corresponding to wavenumbers 1-5 and a period of 20–100 days. In Fig 6 the  
 210 variance of the MJO-filtered daily OLR anomalies is shown. In observations (Fig 6a), the peak  
 211 variance is over the Indo-Pacific warm pool. Feeble variance peaks are noted in the eastern sides  
 212 of the Pacific (off the Gulf of California) and Atlantic (around the western coast of Sierra Leone).  
 213 It is consistent with the fact that although MJO is most active in the Indo-Pacific warm pool re-  
 214 gion, it has considerable influence modulating the convective activity over the eastern equato-  
 215 rial Pacific [Maloney and Hartmann, 2000a,b; Maloney and Kiehl, 2002] and Atlantic [Klotzbach,  
 216 2014]. For  $EXPT_{fast}$  high variance is noted around the warm-pool region but widely spread and  
 217 has multiple peaks. The strongest variance is around Northern Australia and the south-western  
 218 Pacific region. The other secondary maxima are over the southern Bay of Bengal, the central equa-  
 219 torial Indian Ocean, and the central Pacific regions.

220 The simulated MJO variance strength and pattern experience some changes with changes  
 221 in  $\tau$  values. In general, a slower  $\tau_O$  keeping  $\tau_L$  same yields more variance. In other words, it in-

222 creases convective activity in MJO space and time scales. In  $EXPT_{2h}$  a pronounced peak is  
 223 located over the western-central equatorial Pacific with two secondary maxima near the south-western  
 224 equatorial Pacific and eastern equatorial Indian Ocean. In  $EXPT_{3h}$  the variance is more concen-  
 225 trated over the western equatorial Pacific, with a secondary peak south of the central equatorial  
 226 Indian Ocean. With larger values of  $\tau_L$ , the maximum variance gets more and more focused over  
 227 the warm pool region, from  $EXPT_{fast}$  to  $EXPT_{3h}$  (comparing Fig 6b-d). It is noteworthy, that  
 228 all the pronounced peaks for  $EXPT_{2h}$  and  $EXPT_{3h}$  are over oceans, in and around the Indo-Pacific  
 229 warm pool region, but split unlike observations (Fig 6a). The model simulated MJO variance fur-  
 230 ther slowing  $\tau_O$  to 4 hours ( $EXPT_{4h}$  shown in Fig 6e) suggests that MJO variance does not nec-  
 231 essarily increase with increasing  $\tau_O$ . The variance peak intensities are visibly weaker in  $EXPT_{04}$   
 232 compared to that in  $EXPT_{2h}$  and  $EXPT_{3h}$  and more only than that in  $EXPT_{fast}$ . However, a note-  
 233 worthy feature of  $EXPT_{4h}$ , a fine detail missing in all other simulations, is the variance peaks  
 234 near the eastern side of the equatorial Pacific and Atlantic oceans. Baring these subtle variance  
 235 peaks,  $EXPT_{slow}$  looks the best, although still a considerably weaker variance peak compared  
 236 to observations. The variance fields normalized by the respective domain means are available  
 237 in Supplementary Fig S4, which depicts a better visual illustration of the variance peaks.

238 A prominent feature of MJOs is eastward propagation. The propagation features of the MJO  
 239 are arguably better characterized by Hovmöller plots averaged over the latitude band between  $10^\circ\text{S}$   
 240 and  $10^\circ\text{N}$ , shown in Fig 7. Each frame in Fig 7 depicts  $10^\circ\text{S}$ - $10^\circ\text{N}$  averaged cross-correlations  
 241 of OLR anomalies with MJO-index. The MJO-index is defined as the 20-100-day filtered OLR  
 242 anomalies averaged over  $5^\circ\text{S}$ - $5^\circ\text{N}$ ,  $75^\circ\text{E}$ - $85^\circ\text{E}$  following *Guo et al. [2015]*. It is noteworthy to  
 243 mention, reiterating *Guo et al. [2015]*, the philosophy behind using such an MJO index. An in-  
 244 dex based on a 20-100 day filter brings out the dominant intraseasonal signal in the data that ide-  
 245 ally should be an MJO signal. The eastward propagating red and blue patches of correlation val-  
 246 ues in observations (Fig 7a) confirm it. We note the phase speed is faster over the west Pacific  
 247 (east of  $\sim 120^\circ\text{E}$ ) than that over the Indian Ocean (west of  $\sim 100^\circ\text{E}$ ). The relatively slow phase speed  
 248 in the longitude range  $\sim 100^\circ$ - $120^\circ\text{E}$  is collocated with the Indonesian archipelago. These dif-  
 249 ferent phase speeds over land and oceanic regions are consistent with MJO interaction with the  
 250 profound diurnal variations of meteorology over the MC. It furthermore emphasizes the need to  
 251 mimic land-ocean heterogeneity realistically in climate models.

252 To assess the performance of our different experiments in simulating MJO propagation fea-  
 253 tures, we recall the "good" and "bad" models of *Guo et al. [2015]*. In Figure 2, *Guo et al. [2015]*  
 254 showed that the "good" models simulated more realistic eastward propagation than the "bad" mod-

255 els. In Fig 7,  $EXPT_{4h}$  is the only experiment with an eastward propagation and exhibits some  
 256 resemblance with observations and the only "good" model, albeit with some key caveats. The  
 257 positive anomalies almost abruptly died over the MC and reappeared over the western Pacific.  
 258 Nonetheless, an intriguing observation, that contains the novelty of our research, is the more re-  
 259 alistic eastward propagation simulated in  $EXPT_{4h}$  than in  $EXPT_{slow}$ . An improved simulation  
 260 of eastward propagation in  $EXPT_{4h}$  supports our argument that using two  $\tau$ s for land and ocean  
 261 is a logical choice. It reconfirms our anticipation that representing land-ocean heterogeneity via  
 262  $\tau$  in ZM in CAM alters convective memory and affects the organization of convection. A larger  
 263  $\tau_O$  than  $\tau_L$ , although reasonable, is only based on intuition. Detailed sensitivity analysis would  
 264 be needed to investigate and pin down the best pair of  $\tau$  values.

#### 265 **4 Discussion and Conclusion**

266 Climate models continue to grow, fueled by a growing understanding of the earth system.  
 267 Hence, it is only logical to include a fairly well-recognized and relatively old knowledge about  
 268 land and ocean heterogeneity of atmospheric convection in the parameterization of convection.  
 269 We argue that using two different  $\tau$  in ZM in CAM can be one simple yet fruit-bearing way. In  
 270 our experiments to investigate the model response to land-ocean heterogeneity in  $\tau$  values, we  
 271 used  $\tau_L = 1$  hr, and  $\tau_O = 2$  hrs, 3 hrs, 4 hrs. In two additional experiments,  $EXPT_{fast}$  and  $EXPT_{slow}$ ,  
 272 we used  $\tau_L = \tau_O = 1$  hr and  $\tau_L = \tau_O = 4$  hrs, respectively, to complement the previous group  
 273 of experiments. The  $\tau$  values that we have used are informed by our knowledge of frequency, life-  
 274 cycle, and behavior of atmospheric convection over land and ocean learned from previous stud-  
 275 ies [Lucas *et al.*, 1994; Williams and Stanfill, 2002; Zipser *et al.*, 2006; Hagos *et al.*, 2013; Mat-  
 276 sui *et al.*, 2016; Roca *et al.*, 2017; Roca and Fiolleau, 2020] and inspired by results of relevant  
 277 model sensitivity experiments [Zhang and McFarlane, 1995; Lee *et al.*, 2009; Mishra and Srini-  
 278 vasan, 2010; Mishra, 2011; Misra *et al.*, 2012].

279 Our findings regarding the model simulated mean state in different experiments are con-  
 280 sistent with earlier studies [Lee *et al.*, 2009; Mishra and Srinivasan, 2010; Mishra, 2011; Misra  
 281 *et al.*, 2012]. For example, total rainfall remained approximately the same while large-scale rain-  
 282 fall increased and convective rain decreased for longer  $\tau_L$ s. Consistency of the model response  
 283 for a slow  $\tau$  only over the oceans with slowing down  $\tau$  globally is most likely a result of 75% of  
 284 the global surface being ocean. However, since there is no physical barrier between the atmospheric  
 285 columns over continents and oceans, having two  $\tau$  values in our experiments, which essentially  
 286 are prescribed to represent heterogeneity in the persistence of convection over the two different

287 surfaces, created a distinction between the intensities with which the model responses are felt over  
288 land and ocean. For example, the oceanic boundary layer is moister and warmer than the con-  
289 tinental boundary layer (Fig 3). Furthermore, the mid-troposphere is drier and cooler over oceans  
290 than over the continents (Fig 2). These land-ocean heterogeneities inevitably create differences  
291 in atmospheric instabilities. These instabilities are essentially realized in the form of atmospheric  
292 convection that, by design in our experiments with slower  $\tau$ , takes longer to bring the atmosphere  
293 back to a background state. It is suggestive of a longer persistence of convective instability over  
294 the ocean than that over the continents which essentially can be linked with memory of convec-  
295 tion [Davies *et al.*, 2009; Colin *et al.*, 2019; Hwong *et al.*, 2023].

296 The conclusion that the model simulated better convectively coupled equatorial waves in  
297  $EXPT_{2h}$  than in  $EXPT_{slow}$  is a key. We conclude this based on our finding of a better MJO sim-  
298 ulation in  $EXPT_{2h}$ , consistent with improved symmetric waves. Scientists had advocated in fa-  
299 vor of a slower  $\tau$  in earlier studies [Mishra, 2011; Misra *et al.*, 2012]. We also noted a signifi-  
300 cant increase in MJO power for  $\tau = 4$  hrs than  $\tau = 1$  hr (comparing Fig 5b and Fig 5f). However,  
301 an evaluation of the model simulated intraseasonal zonal propagation reveals that  $EXPT_{4h}$  per-  
302 forms considerably better than  $EXPT_{slow}$ . This confirms that having one  $\tau$  globally is not only  
303 unphysical but also slowing down tinkering persistence of convection to improve simulation of  
304 equatorial waves, and may result in model responses that might look improved, but only super-  
305 ficially.

306 Our results, in general, serve as proof of concept that a realistic representation of convec-  
307 tive adjustment time scale over land and ocean is a logical requirement that properly implemented  
308 shall lead to improvements in climate model simulations. In specific, we advocate at least two  
309  $\tau$  values, one for the continents and one relatively slower for the oceans in ZM in CAM. The fact  
310 that we did not perform a rigorous model sensitivity analysis [e.g., Qian *et al.*, 2015; Lin *et al.*,  
311 2016; Goswami *et al.*, 2017] nor did we perform any cloud-resolving simulation targeting the  
312 life-cycle of atmospheric convection [Davies *et al.*, 2013; Colin *et al.*, 2019; Daleu *et al.*, 2020,  
313 e.g.,] leaves a scope as well as the requirement for future research to determine the best values  
314 of  $\tau_L$  and  $\tau_O$  for ZM in CAM. It will hopefully guide convection parameterization schemes, es-  
315 pecially the adjustment types, to address land-ocean heterogeneity. Specifically, we recommend  
316 that future developments of CAM should consider prescribing different  $\tau_L$  and  $\tau_O$  in ZM in CAM.

## 5 Open Research

- 318 • Model : We used the atmospheric model of the Community Earth System Model, version  
319 2.1.3 (CESM 2.1.3) [Danabasoglu *et al.*, 2020]
- 320 • Description of the model simulations is provided in Section 2 of the manuscript. A source  
321 file of CESM 2.1.3, zm\_conv.F90, modified for our experiments is provided in [https://github.com/bidyutbg/CESM\\_Tau\\_experiment.git](https://github.com/bidyutbg/CESM_Tau_experiment.git).  
322
- 323 • Data analysis software: Figures 1-5 are produced in Python and the details of the method-  
324 ology is provided in the relevant sections of the text. Figure 5 is produced using script avail-  
325 able at [https://github.com/bidyutbg/CESM\\_Tau\\_experiment/blob/main/WK\\_spectra\\_FINAL-NEW.ipynb](https://github.com/bidyutbg/CESM_Tau_experiment/blob/main/WK_spectra_FINAL-NEW.ipynb). Figure 6 is produced using script available at [https://github.com/bidyutbg/CESM\\_Tau\\_experiment/blob/main/CCEW\\_variance-compare\\_FINAL.ipynb](https://github.com/bidyutbg/CESM_Tau_experiment/blob/main/CCEW_variance-compare_FINAL.ipynb). Figure 7 is produced using script available at [https://www.ncl.ucar.edu/Applications/Scripts/mjoclivar\\_9.ncl](https://www.ncl.ucar.edu/Applications/Scripts/mjoclivar_9.ncl).  
326  
327  
328  
329
- 330 • Model Output Data: Data archival is underway in Zenodo. Archival will be completed  
331 soon. A sample of the data is provided as Supporting Information for review purposes.

## Acknowledgments

332 The authors gratefully acknowledge funding from the European Research Council (ERC) under  
333 the European Union’s Horizon 2020 research and innovation program (Project CLUSTER, Grant  
334 Agreement No. 805041). This research was supported by the Scientific Service Units (SSU) of  
335 ISTA through resources provided by Scientific Computing (SciComp).  
336

## References

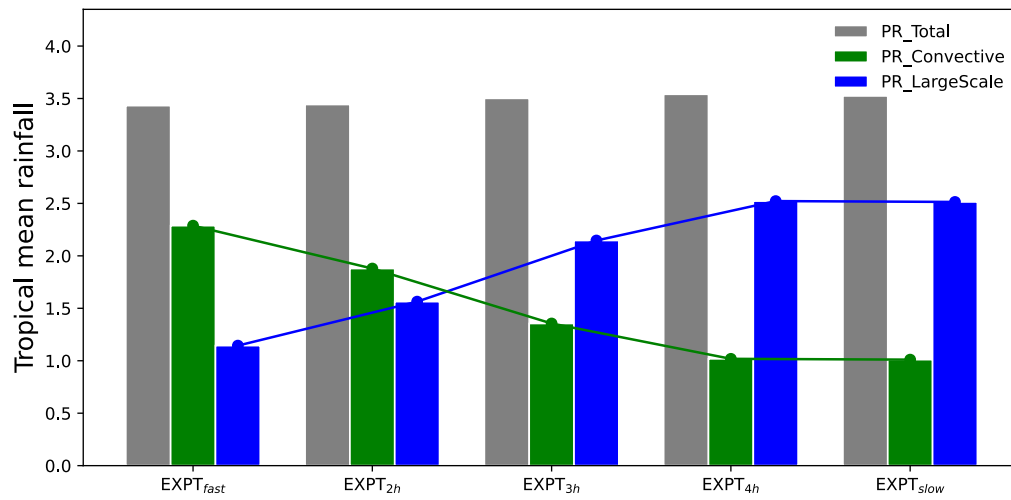
- 337
- 338 Arakawa, A. (2004), The Cumulus Parameterization Problem: Past, Present, and Future,  
339 *Journal of Climate*, 17(13), 2493–2525, doi:10.1175/1520-0442(2004)017<2493:  
340 RATCPP>2.0.CO;2.
- 341 Colin, M., S. Sherwood, O. Geoffroy, S. Bony, and D. Fuchs (2019), Identifying the Sources  
342 of Convective Memory in Cloud-Resolving Simulations, *Journal of the Atmospheric*  
343 *Sciences*, 76(3), 947–962, doi:10.1175/JAS-D-18-0036.1.
- 344 Daleu, C. L., R. S. Plant, S. J. Woolnough, A. J. Stirling, and N. J. Harvey (2020), Memory  
345 Properties in Cloud-Resolving Simulations of the Diurnal Cycle of Deep Convection,  
346 *Journal of Advances in Modeling Earth Systems*, 12(8), doi:10.1029/2019MS001897.

- 347 Danabasoglu, G., J. Lamarque, J. Bacmeister, D. A. Bailey, A. K. DuVivier, J. Edwards,  
348 L. K. Emmons, J. Fasullo, R. Garcia, A. Gettelman, C. Hannay, M. M. Holland, W. G.  
349 Large, P. H. Lauritzen, D. M. Lawrence, J. T. M. Lenaerts, K. Lindsay, W. H. Lipscomb,  
350 M. J. Mills, R. Neale, K. W. Oleson, B. Otto-Bliesner, A. S. Phillips, W. Sacks, S. Tilmes,  
351 L. Kampenhout, M. Vertenstein, A. Bertini, J. Dennis, C. Deser, C. Fischer, B. Fox-  
352 Kemper, J. E. Kay, D. Kinnison, P. J. Kushner, V. E. Larson, M. C. Long, S. Mickelson,  
353 J. K. Moore, E. Nienhouse, L. Polvani, P. J. Rasch, and W. G. Strand (2020), The Com-  
354 munity Earth System Model Version 2 (CESM2), *Journal of Advances in Modeling Earth*  
355 *Systems*, 12(2), doi:10.1029/2019MS001916.
- 356 Davies, L. (2008), Self-organisation of convection as a mechanism for memory, Ph.D. thesis,  
357 The University of Reading.
- 358 Davies, L., R. S. Plant, and S. H. Derbyshire (2009), A simple model of convection with  
359 memory, *Journal of Geophysical Research: Atmospheres*, 114(D17), 17,202, doi:  
360 10.1029/2008JD011653.
- 361 Davies, L., R. S. Plant, and S. H. Derbyshire (2013), Departures from convective equilibrium  
362 with a rapidly varying surface forcing, *Quarterly Journal of the Royal Meteorological*  
363 *Society*, 139(676), 1731–1746, doi:10.1002/qj.2065.
- 364 Goswami, B. B., B. Khouider, R. Phani, P. Mukhopadhyay, and A. J. Majda (2017),  
365 Implementation and calibration of a stochastic multcloud convective parameteriza-  
366 tion in the NCEP <sc>C</sc> limate <sc>F</sc> orecast <sc>S</sc> ystem  
367 (CFSv2), *Journal of Advances in Modeling Earth Systems*, 9(3), 1721–1739, doi:  
368 10.1002/2017MS001014.10.1002/2017MS001014.
- 369 Guo, Y., D. E. Waliser, and X. Jiang (2015), A Systematic Relationship between the Rep-  
370 resentations of Convectively Coupled Equatorial Wave Activity and the Madden–Julian  
371 Oscillation in Climate Model Simulations, *Journal of Climate*, 28(5), 1881–1904, doi:  
372 10.1175/JCLI-D-14-00485.1.10.1175/JCLI-D-14-00485.1.
- 373 Hagos, S., Z. Feng, S. Mcfarlane, and L. R. Leung (2013), Environment and the Lifetime of  
374 Tropical Deep Convection in a Cloud-Permitting Regional Model Simulation, *Journal of*  
375 *the Atmospheric Sciences*, 70(8), 2409–2425, doi:10.1175/JAS-D-12-0260.1.
- 376 Hourdin, F., T. Mauritsen, A. Gettelman, J. C. Golaz, V. Balaji, Q. Duan, D. Folini, D. Ji,  
377 D. Klocke, Y. Qian, F. Rauser, C. Rio, L. Tomassini, M. Watanabe, and D. Williamson  
378 (2017), The Art and Science of Climate Model Tuning, *Bulletin of the American Meteorolo-*  
379 *logical Society*, 98(3), 589–602, doi:10.1175/BAMS-D-15-00135.1.

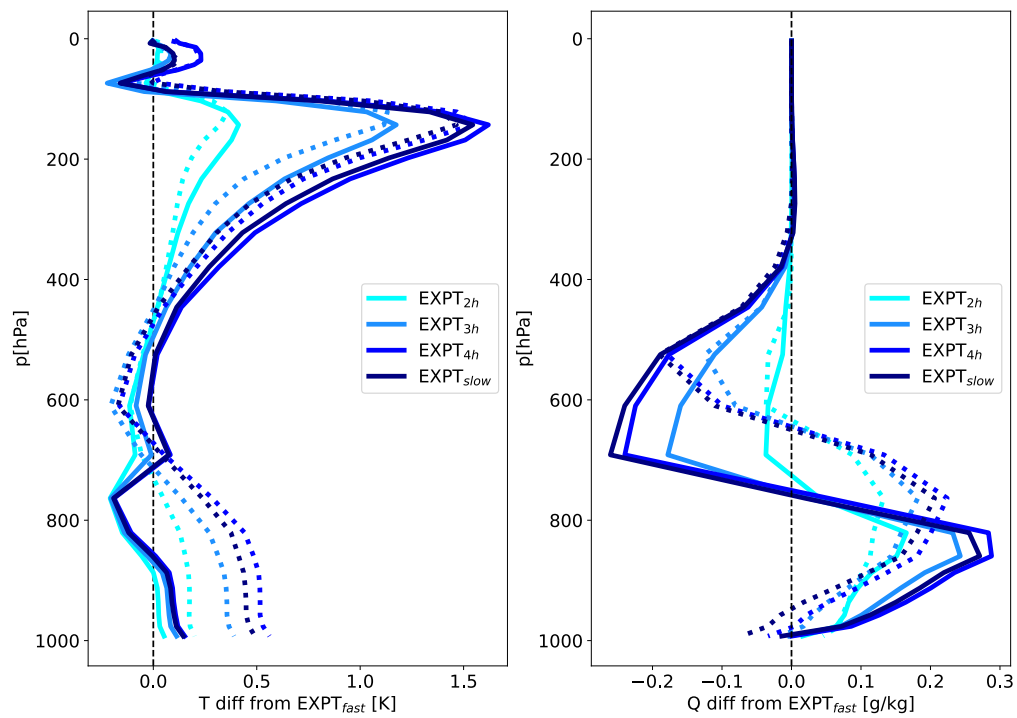
- 380 Hwong, Y.-L., M. Colin, P. Aglas-Leitner, C. Muller, and S. Sherwood (2023), Assessing  
381 Memory in Convection Schemes Using Idealized Tests, *ESS Open Archive*, preprint.
- 382 Klotzbach, P. J. (2014), The Madden–Julian Oscillation’s Impacts on Worldwide Tropical  
383 Cyclone Activity, *Journal of Climate*, 27(6), 2317–2330, doi:10.1175/JCLI-D-13-00483.  
384 1.
- 385 Lee, J. E., R. Pierrehumbert, A. Swann, and B. R. Lintner (2009), Sensitivity of stable water  
386 isotopic values to convective parameterization schemes, *Geophysical Research Letters*,  
387 36(23), doi:10.1029/2009GL040880.
- 388 Liebmann, B., and C. Smith (1996), Description of a Complete (Interpolated) Outgoing  
389 Longwave Radiation Dataset., *Bulletin of the American Meteorological Society*, 77, 1275–  
390 1277.
- 391 Lin, G., H. Wan, K. Zhang, Y. Qian, and S. J. Ghan (2016), Can nudging be used to quantify  
392 model sensitivities in precipitation and cloud forcing?, *Journal of Advances in Modeling  
393 Earth Systems*, 8(3), 1073–1091, doi:10.1002/2016MS000659.
- 394 Lucas, C., E. J. Zipser, and M. A. Lemone (1994), Vertical Velocity in Oceanic Convec-  
395 tion off Tropical Australia, *Journal of the Atmospheric Sciences*, 51(21), 3183–3193,  
396 doi:10.1175/1520-0469(1994)051<3183:VVIOCO>2.0.CO;2.
- 397 Maloney, E. D., and D. L. Hartmann (2000a), Modulation of Eastern North Pacific Hur-  
398 ricanes by the Madden–Julian Oscillation, *Journal of Climate*, 13(9), 1451–1460, doi:  
399 10.1175/1520-0442(2000)013<1451:MOENPH>2.0.CO;2.
- 400 Maloney, E. D., and D. L. Hartmann (2000b), Modulation of Hurricane Activity in the  
401 Gulf of Mexico by the Madden-Julian Oscillation, *Science*, 287(5460), 2002–2004, doi:  
402 10.1126/science.287.5460.2002.
- 403 Maloney, E. D., and J. T. Kiehl (2002), MJO-Related SST Variations over the Tropical East-  
404 ern Pacific during Northern Hemisphere Summer, *Journal of Climate*, 15(6), 675–689,  
405 doi:10.1175/1520-0442(2002)015<0675:MRSVOT>2.0.CO;2.
- 406 Matsui, T., J. D. Chern, W. K. Tao, S. Lang, M. Satoh, T. Hashino, and T. Kubota (2016),  
407 On the Land–Ocean Contrast of Tropical Convection and Microphysics Statistics Derived  
408 from TRMM Satellite Signals and Global Storm-Resolving Models, *Journal of Hydrome-  
409 teorology*, 17(5), 1425–1445, doi:10.1175/JHM-D-15-0111.1.
- 410 Mishra, S. K. (2011), Influence of convective adjustment time scale on the tropi-  
411 cal transient activity, *Meteorology and Atmospheric Physics*, 114(1), 17–34, doi:  
412 10.1007/S00703-011-0154-8/FIGURES/19.

- 413 Mishra, S. K. (2012), Effects of convective adjustment time scale on the simulation  
414 of tropical climate, *Theoretical and Applied Climatology*, *107*(1-2), 211–228, doi:  
415 10.1007/S00704-011-0479-8/FIGURES/19.
- 416 Mishra, S. K., and J. Srinivasan (2010), Sensitivity of the simulated precipitation to changes  
417 in convective relaxation time scale, *Annales Geophysicae*, *28*(10), 1827–1846, doi:  
418 10.5194/ANGE0-28-1827-2010.
- 419 Misra, V., P. Pantina, S. Chan, and S. DiNapoli (2012), A comparative study of the Indian  
420 summer monsoon hydroclimate and its variations in three reanalyses, *Climate Dynamics*,  
421 *39*(5), 1149–1168, doi:10.1007/s00382-012-1319-y.
- 422 Qian, Y., H. Yan, Z. Hou, G. Johannesson, S. Klein, D. Lucas, R. Neale, P. Rasch,  
423 L. Swiler, J. Tannahill, H. Wang, M. Wang, and C. Zhao (2015), Parametric sensitiv-  
424 ity analysis of precipitation at global and local scales in the Community Atmosphere  
425 Model CAM5, *Journal of Advances in Modeling Earth Systems*, *7*(2), 382–411, doi:  
426 10.1002/2014MS000354.
- 427 Randall, D., M. Khairoutdinov, A. Arakawa, and W. Grabowski (2003), Breaking the Cloud  
428 Parameterization Deadlock, *Bulletin of the American Meteorological Society*, *84*(11),  
429 1547–1564, doi:10.1175/BAMS-84-11-1547.
- 430 Randall, D. A. (2013), Beyond deadlock, *Geophysical Research Letters*, *40*(22), 5970–5976,  
431 doi:10.1002/2013GL057998.
- 432 Rayner, N. A. (2003), Global analyses of sea surface temperature, sea ice, and night ma-  
433 rine air temperature since the late nineteenth century, *Journal of Geophysical Research*,  
434 *108*(D14), doi:10.1029/2002JD002670.
- 435 Rio, C., A. D. Del Genio, and F. Hourdin (2019), Ongoing Breakthroughs in Convec-  
436 tive Parameterization, *Current Climate Change Reports 2019 5:2*, *5*(2), 95–111, doi:  
437 10.1007/S40641-019-00127-W.
- 438 Roca, R., and T. Fiolleau (2020), Extreme precipitation in the tropics is closely associated  
439 with long-lived convective systems, *Communications Earth & Environment 2020 1:1*,  
440 *1*(1), 1–6, doi:10.1038/s43247-020-00015-4.
- 441 Roca, R., T. Fiolleau, and D. Bouniol (2017), A Simple Model of the Life Cycle of  
442 Mesoscale Convective Systems Cloud Shield in the Tropics, *Journal of Climate*, *30*(11),  
443 4283–4298, doi:10.1175/JCLI-D-16-0556.1.
- 444 Stevens, B., M. Satoh, L. Auger, J. Biercamp, C. S. Bretherton, X. Chen, P. Düben, F. Judt,  
445 M. Khairoutdinov, D. Klocke, C. Kodama, L. Kornbluh, S. J. Lin, P. Neumann, W. M.

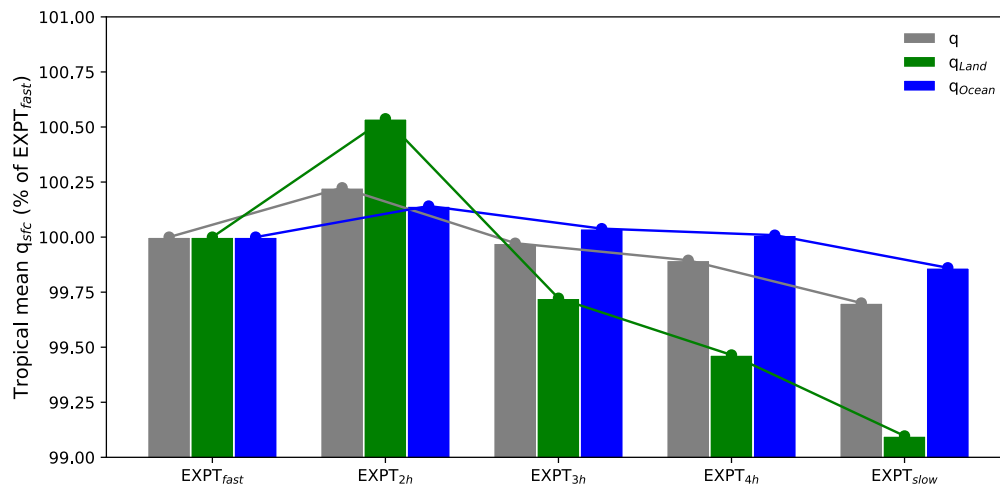
- 446 Putman, N. Röber, R. Shibuya, B. Vanniere, P. L. Vidale, N. Wedi, and L. Zhou (2019),  
447 DYAMOND: the DYnamics of the Atmospheric general circulation Modeled On  
448 Non-hydrostatic Domains, *Progress in Earth and Planetary Science*, 6(1), 1–17, doi:  
449 10.1186/S40645-019-0304-Z/FIGURES/9.
- 450 Takayabu, Y. (1994a), Large-Scale Cloud Disturbances Associated with Equatorial  
451 Waves, *Journal of the Meteorological Society of Japan. Ser. II*, 72(3), 433–449, doi:  
452 10.2151/jmsj1965.72.3{\\_}433.
- 453 Takayabu, Y. (1994b), Large-Scale Cloud Disturbances Associated with Equatorial  
454 Waves, *Journal of the Meteorological Society of Japan. Ser. II*, 72(3), 451–465, doi:  
455 10.2151/jmsj1965.72.3{\\_}451.
- 456 Wheeler, M., and G. N. Kiladis (1999), Convectively Coupled Equatorial Waves: Anal-  
457 ysis of Clouds and Temperature in the Wavenumber-Frequency Domain, *Journal of*  
458 *the Atmospheric Sciences*, 56(3), 374–399, doi:10.1175/1520-0469(1999)056<0374:  
459 CCEWAO>2.0.CO;2.
- 460 Williams, E., and S. Stanfill (2002), The physical origin of the land-ocean contrast in light-  
461 ning activity, *Comptes Rendus Physique*, 3(10), 1277–1292, doi:10.1016/S1631-0705(02)  
462 01407-X.
- 463 Zhang, C., F. Adames, B. Khouider, B. Wang, and D. Yang (2020), Four Theories of  
464 the Madden-Julian Oscillation, *Reviews of Geophysics*, 58(3), e2019RG000,685, doi:  
465 10.1029/2019RG000685.
- 466 Zhang, G. J., and N. A. McFarlane (1995), Sensitivity of climate simulations to the parame-  
467 terization of cumulus convection in the Canadian climate centre general circulation model,  
468 *Atmosphere-Ocean*, 33(3), 407–446, doi:10.1080/07055900.1995.9649539.
- 469 Zipser, E. J., D. J. Cecil, C. Liu, S. W. Nesbitt, and D. P. Yorty (2006), Where are the most:  
470 Intense thunderstorms on Earth?, *Bulletin of the American Meteorological Society*, 87(8),  
471 1057–1071, doi:10.1175/BAMS-87-8-1057.



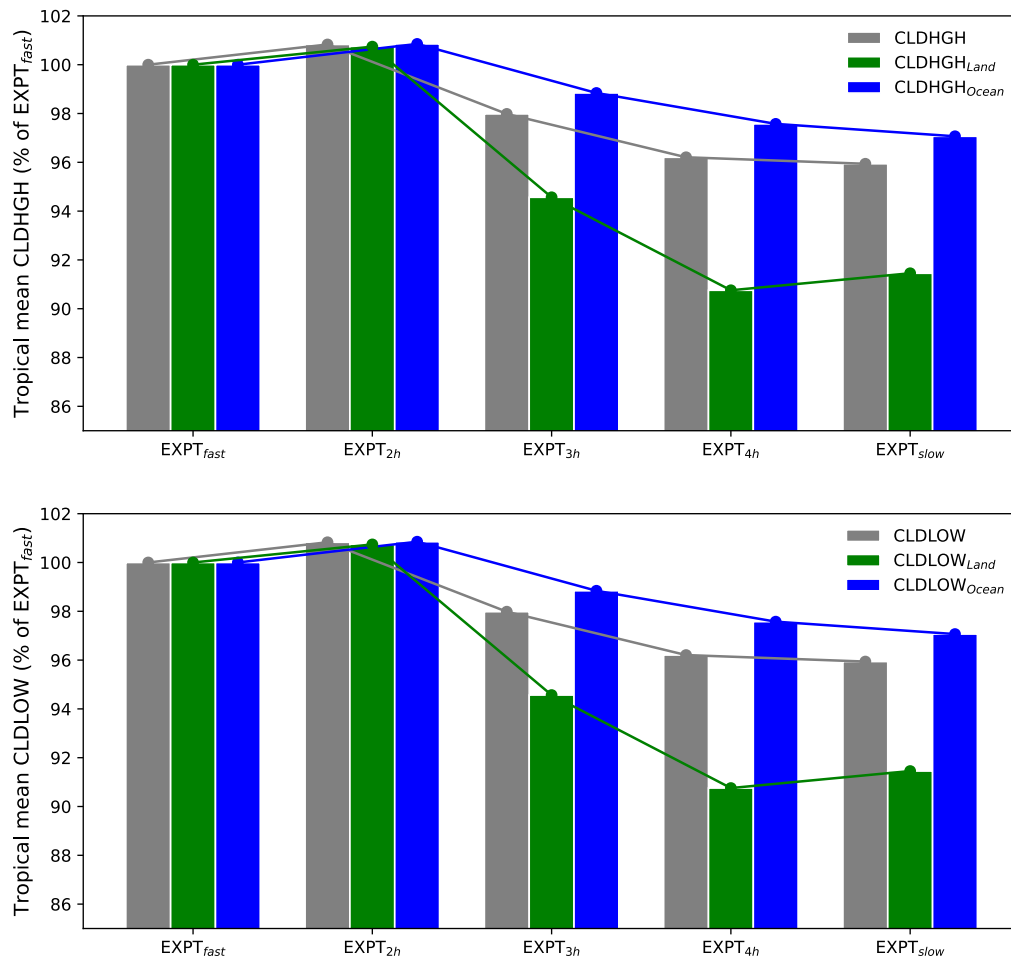
472 **Figure 1.** Tropical (tropics defined as the zonal belt between 30°S-30°N) annual mean daily rainfall  
 473 (mm/day) for different experiments mentioned in Table 1.



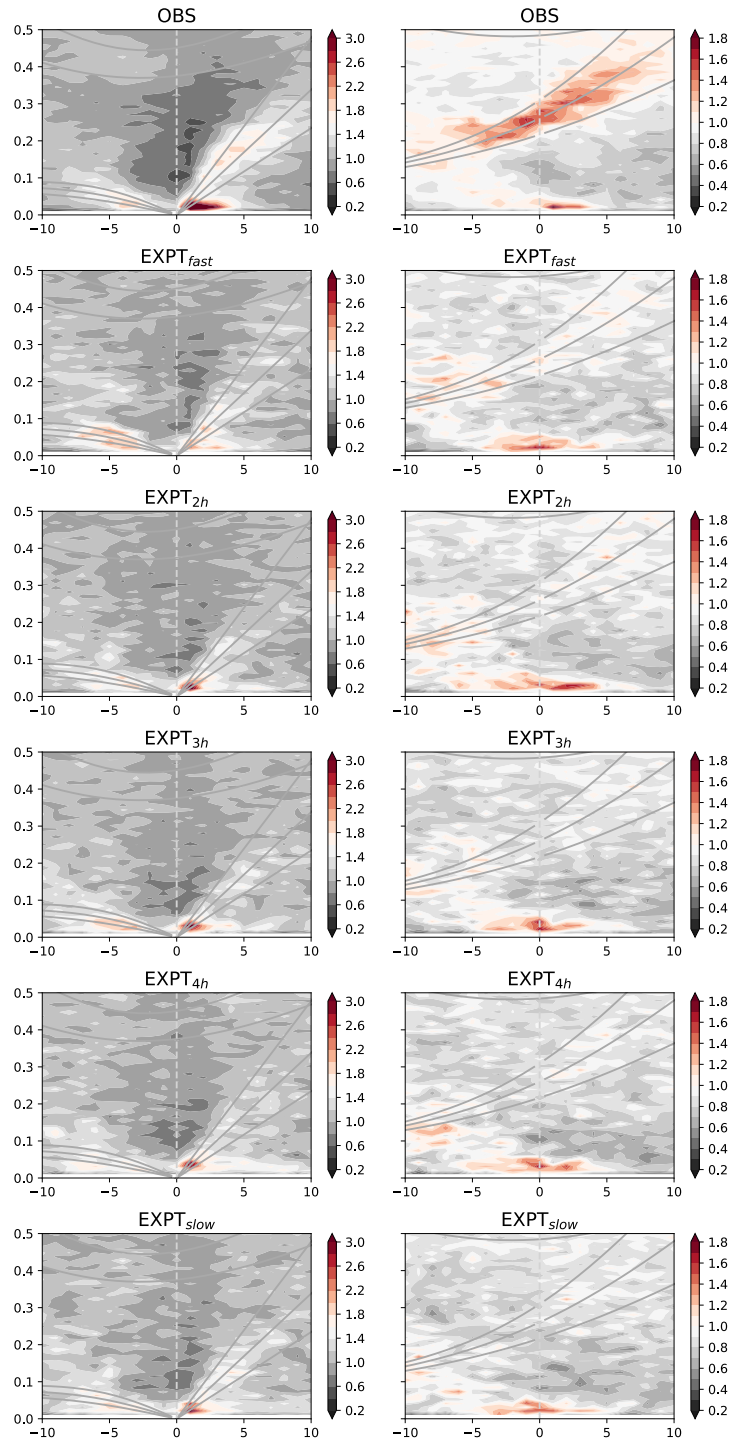
474 **Figure 2.** Tropical (tropics defined as the zonal belt between 30°S-30°N) mean vertical profiles of tem-  
 475 perature (T) and specific humidity (Q). Departures of different experiments, as indicated in the legends, from  
 476  $EXPT_{fast}$  (Land: Dotted, Ocean: Solid). The vertical dashed line indicate the zero line.



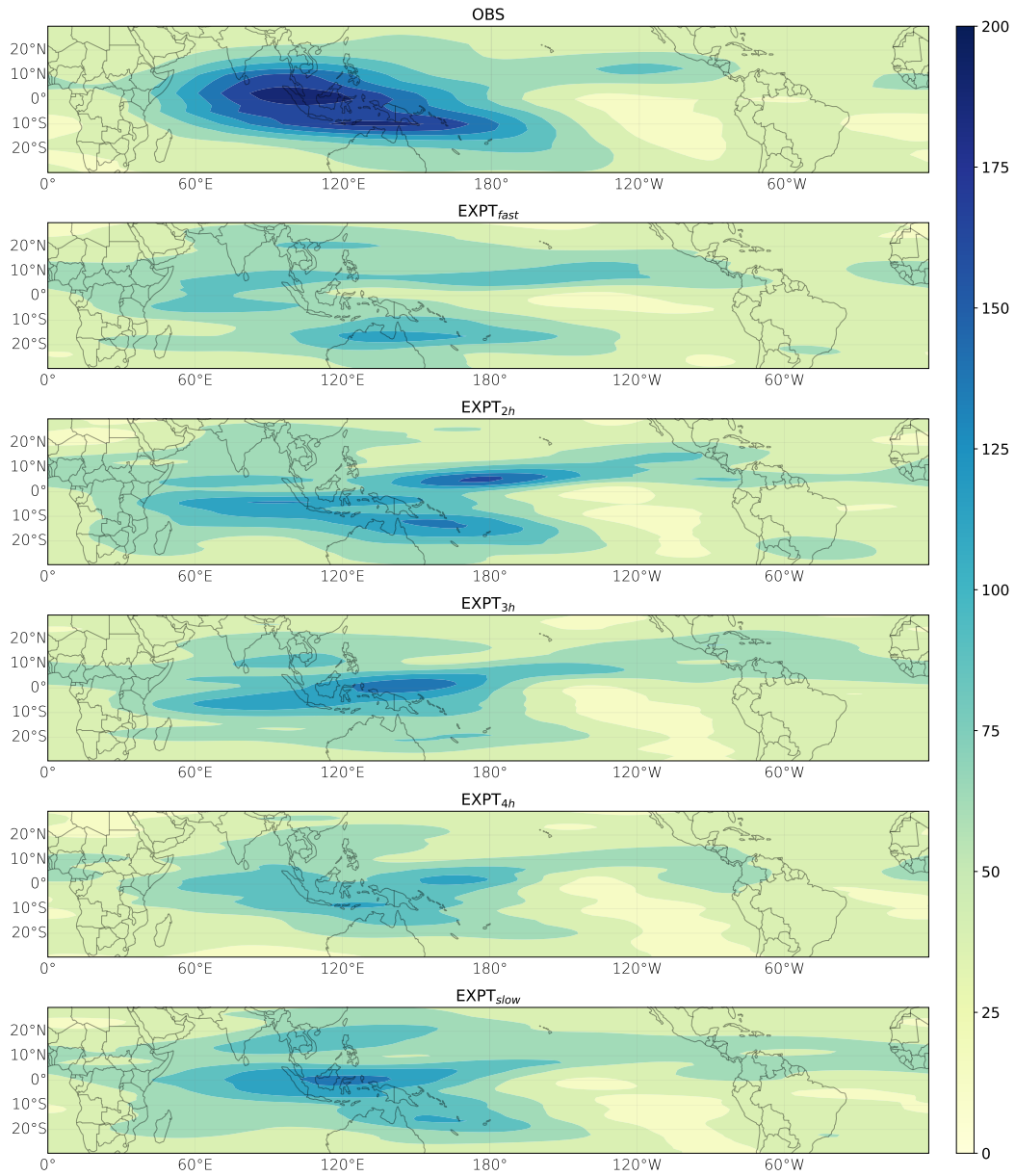
477 **Figure 3.** Tropical (tropics defined as the zonal belt between 30°S-30°N) annual daily mean specific hu-  
 478 midity as surface depicted as % of  $EXPT_{fast}$ .



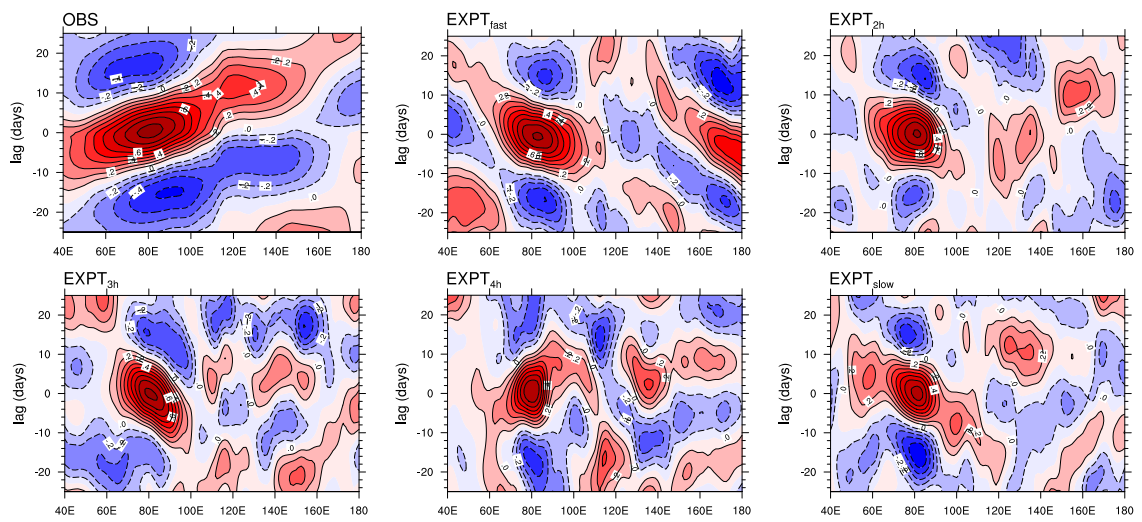
479 **Figure 4.** Tropical (tropics defined as the zonal belt between 30°S-30°N) annual daily mean High and Low  
 480 cloud cover depicted as % of  $EXPT_{fast}$ .



481 **Figure 5.** Takayabu-Wheeler-Kiladis spectra of OLR for OBS (from NOAA) and different experiments (as  
 482 named above each panel), for the symmetric component (left-hand side panels) and antisymmetric component  
 483 (right-hand side panels).



484 **Figure 6.** MJO variance computed as the daily variance of OLR data filtered for 1-5 wavenumber and 20-  
 485 100 day frequency, for OBS (from NOAA) and different experiments (as named above each panel).



486 **Figure 7.** MJO propagation: Hovmöller (averaged from 10°S to 10°N) plots of MJO-filtered OLR (W m<sup>-2</sup>)  
487 anomalies (Winter), for OBS (from NOAA) and different experiments (as named above each panel).

1           **An assessment of representing land-ocean heterogeneity via**  
2           **convective adjustment timescale in the Community Atmospheric**  
3           **Model 6 (CAM6)**

4           **Bidyut Bikash Goswami<sup>1</sup>, Andrea Polesello<sup>1</sup>, Caroline Muller<sup>1</sup>**

5           <sup>1</sup>Institute of Science and Technology Austria (ISTA), Klosterneuburg, Austria

6           **Key Points:**

- 7           • Two distinct values of convective adjustment timescale,  $\tau$ , over land & ocean in the con-
- 8           convective parameterization scheme are prescribed.
- 9           • The mean climate stays qualitatively the same, except for a moister and colder near-surface
- 10          atmosphere for longer  $\tau$ s over the oceans.
- 11          • A primary gain of using two different  $\tau$ s for land and ocean is improved simulation of the
- 12          convectively coupled equatorial waves.

---

Corresponding author: B. B. Goswami, [bgoswami@ista.ac.at](mailto:bgoswami@ista.ac.at)

## Abstract

The time needed by deep convection to bring the atmosphere back to equilibrium is called convective adjustment timescale or simply adjustment timescale, typically denoted by  $\tau$ . In the Community Atmospheric Model (CAM), convective adjustment timescale is a tunable parameter with one value, 1 hour, worldwide. Albeit, there is no justified reason why one adjustment timescale value should work over land and ocean both. Continental and oceanic convection are different in terms of the vigor of updrafts and hence can have different longevities. So it is logical to investigate the prescription of two different convective adjustment timescales for land ( $\tau_L$ ) and ocean ( $\tau_O$ ). To understand the impact of representing land-ocean heterogeneity via  $\tau$ , we investigate CAM climate simulations for two different convective adjustment timescales for land and ocean in contrast to having one value globally.

Following a comparative analysis of 5-year-long climate simulations, we find  $\tau_O = 4$  hrs and  $\tau_L = 1$  hr to yield the best results. Particularly, we find better MJO simulations. Although these  $\tau$  values were chosen empirically and require further tuning, the conclusion of our finding remains the same, which is the recommendation to use two different  $\tau$  values for land and ocean.

## 1 Introduction

Deep convection is complex to parameterize [Arakawa, 2004]. While the explicit representation of deep convection is becoming a plausible option to navigate this "deadlock" [Randall *et al.*, 2003; Randall, 2013], for long-term projections of our climate, cumulus parameterization is still unavoidable. Hence, amidst the fierce emergence of convection-resolving models [Stevens *et al.*, 2019], various schemes to parameterize convection continue to develop. In particular, the recent decades have witnessed a surge of novel ideas that have accelerated this progress [Rio *et al.*, 2019, and references therein].

The "art" of tuning parameters used in convection parameterization schemes, or simply parameter tuning, plays a vital role in this development process [Hourdin *et al.*, 2017]. While deficiencies of convective parameterization are primary factors for model biases, it alone cannot alleviate all mode biases [Goswami *et al.*, 2017]. Hence, parameter sensitivity investigations are necessary not only to optimize the performance of a scheme but also to understand the extremities to which a scheme can be held responsible for biases in a simulation [Qian *et al.*, 2015; Goswami *et al.*, 2017]. In this study, we aim to contribute to understanding one tunable parameter, the convective adjustment timescale  $\tau$ , by investigating the sensitivity of climate simulations to two dif-

44 ferent  $\tau$  values for land and ocean in contrast to having one value globally in the Zhang-McFarlane  
45 convective parameterization scheme [Zhang and McFarlane, 1995, ZM95 hereafter] in the Com-  
46 munity Atmospheric Model (CAM), the atmospheric model of the Community Earth System Model  
47 [Danabasoglu et al., 2020].

48 In CAM, deep convection is represented using the Zhang-McFarlane (ZM) convection pa-  
49 rameterization scheme. The ZM is an adjustment-type convective parameterization scheme where  
50 the atmospheric instability is removed via an adjustment towards a background state. In ZM, con-  
51 vective available potential energy (CAPE) defines atmospheric instability, and  $\tau$  is the CAPE con-  
52 sumption time. In their paper, ZM95 used  $\tau$  values of 2, 4, and 6 hours. To quote ZM95, "The  
53 adjustment time scale determines the intensity and duration of convection for a given CAPE. With  
54 small  $\tau$  the convection is short-lived but intensity is high, on the other hand with larger  $\tau$  the con-  
55 vection is long-lived but of low intensity". ZM95 reported their scheme to be particularly sen-  
56 sitive to the choice of  $\tau$ . Since there is no strict range of  $\tau$ , several studies investigated the sen-  
57 sitivity of CAM simulations to different  $\tau$  values. For example, Mishra and Srinivasan [2010]  
58 used  $\tau=[1,\infty]$ . Contrasting water-vapor isotope simulations in a suite of CAM single-column sim-  
59 ulations with a range of  $\tau$  values, Lee et al. [2009] found their simulations to match better with  
60 satellite observations with  $\tau = 8$  hrs. Mishra [2011, 2012] prescribed  $\tau = 8$  hrs in global climate  
61 simulations and noted improvements in the simulations of tropical climate, especially the con-  
62 vectively coupled equatorial waves. Evaluating 22 tunable parameters in CAM, Qian et al. [2015]  
63 reported  $\tau$  as one of the most critical tuning parameters. In all of the above studies,  $\tau$  has a sin-  
64 gular value globally.

65 One value of  $\tau$  globally is not a logical choice because deep convection exhibits different  
66 behaviors over continents and oceans [Hagos et al., 2013; Matsui et al., 2016; Roca et al., 2017;  
67 Roca and Fiolleau, 2020]. Since the width of a thermal plume is steered by boundary layer height  
68 [Williams and Stanfill, 2002], a deep continental boundary layer generates wider updraft veloc-  
69 ities in deep convection [Lucas et al., 1994]. Matsui et al. [2016] provided a climatological view  
70 of the contrast between oceanic and continental convective precipitating clouds from long-term  
71 TRMM satellite multisensor statistics. They found large proportions of deep clouds over land.  
72 Zipser et al. [2006] also found the most intense storms typically over continents. These obser-  
73 vations suggest that the atmospheric deep convection over land is wider and stronger than those  
74 over the oceans. In other words, atmospheric convection over land is shorter lived than that over  
75 ocean [Roca et al., 2017]. It advocates for a shorter convection consumption time scale over land  
76 than over oceans which motivated us to address the following question: although two different

77  $\tau$  values incorporating land-ocean inhomogeneity are logical, is it fruit-bearing in a model-simulated  
78 climate? To answer this question, we investigate,

- 79 • response of the mean climate, and
- 80 • response of large-scale waves,

81 by contrasting 5-year-long climate simulations with and without incorporating land-ocean inho-  
82 mogeneity via  $\tau$  values.

83 Convective parameterization schemes, particularly adjustment-type schemes, are based on  
84 the idea that convection takes some time to stabilize the atmosphere to a background state. Es-  
85 sentially, this time taken is  $\tau$  in the ZM scheme. Although numerically  $\tau$  can have almost any value,  
86 it is decided based on a scale separation between the convective activity of the individual clouds  
87 and large-scale forcing. This concept is nicely depicted in Figure 1.1 of [Davies, 2008]. The graph  
88 in that figure is a function of timescales associated with convection, and consists of a turbulent  
89 initial segment indicating fluctuation of individual clouds, followed by a flat segment where these  
90 fluctuations smooth out, and finally a segment corresponding to longer time-scales that shows  
91 the evolution of the large scale forcing field itself. Conceptually, changing  $\tau$  within a reasonable  
92 range (within the flat segment of Figure 1.1 of [Davies, 2008]) should not result in a dramatic change  
93 in the mean state of the simulated climate. We shall investigate it in detail in the first part of our  
94 results section.

95 Some changes that we expect in our experiments are in the simulated organization of con-  
96 vection. The organization of convection comes from the dynamic and thermodynamic impacts  
97 of convection on the atmosphere. Simply put, it is the memory of convection [Davies *et al.*, 2009],  
98 i.e. the fact that convection changes the large-scale properties, and can make their environment  
99 favorable or unfavorable to subsequent convection. Identifying sources of convective memory  
100 in cloud-resolving simulations, Colin *et al.* [2019] argued that the persistence of the state of con-  
101 vection contributes to convective memory. Colin *et al.* [2019] also suggested that convective mem-  
102 ory and organization interact mutually. By altering  $\tau$  we essentially alter memory associated with  
103 convection. Hence, we expect to see changes in convective organization. Taking a cue from Mishra  
104 [2011], we anticipate improved convective organization in the tropics for longer  $\tau$ . However, land-  
105 ocean heterogeneity in  $\tau$  is a unique feature of our experiments that we argue is essential based  
106 on heterogeneity in the behavior of convection over land and ocean. As supporting evidence, we

107 shall present an analysis of equatorial waves focusing on the MJO to evaluate the organization  
 108 of convection in the second part of our results section.

109 The paper is organized as follows. A brief description of the methodology is provided in  
 110 Section 2. Section 3 evaluates the response of the model to different  $\tau$  values. Finally, a few con-  
 111 cluding remarks are provided in Section 4.

## 112 **2 Model and simulation details**

113 We used the atmospheric model of the Community Earth System Model, version 2.1.3 (CESM  
 114 2.1.3) [Danabasoglu *et al.*, 2020], that is the Community Atmosphere Model, version 6 (CAM6),  
 115 developed and maintained at the National Center for Atmospheric Research (NCAR), with lon-  
 116 gitude and latitude specifications  $1.25^\circ$  and  $0.9^\circ$ , respectively, and 32 vertical levels. We forced  
 117 the model by HadISST1 climatological monthly mean SST data provided by the Met Office Hadley  
 118 Centre [Rayner, 2003]. In short, we performed CESM “F2000climo” simulations. In general,  
 119 these are atmospheric simulations forced by present-day climatology. All simulations are 6 years  
 120 long, and we analyzed the last 5 years of each simulation since, for atmosphere-only simulations,  
 121 1-year spin-up is enough.

122 We performed 5 simulations. The one with out-of-the-box  $\tau$  value of 1 hour globally is called  
 123 the control (*CTRL*). In the next 3 simulations, we delayed the  $\tau$  value over ocean ( $\tau_O$ ) to 2, 3 and  
 124 4 hours keeping  $\tau$  over land ( $\tau_L$ ) 1 hour. We called these 3 simulations *EXPT<sub>2h</sub>*, *EXPT<sub>3h</sub>* and  
 125 *EXPT<sub>4h</sub>*, respectively. We performed a last 5<sup>th</sup> experiment, named *EXPT<sub>slow</sub>*, for which we used  
 126 a  $\tau$  value of 4 hours globally. Before starting our comparative analysis, we rename our first sim-  
 127 ulation as *EXPT<sub>fast</sub>*, which initially we had named CTRL, for clarity and better fluency of nar-  
 128 ration of our findings. Table 1 depicts the  $\tau$  values for different experiments.

129 Our analyses primarily show a comparison between the 5 aforementioned simulations. For  
 130 some analyses we have used outgoing long-wave radiation (OLR) from NOAA ( $2.5^\circ \times 2.5^\circ$ ; daily  
 131 from 01-Jun-1974 to 12-Dec-2019) [Liebmann and Smith, 1996] as observational benchmark.

## 133 **3 Results**

### 134 **3.1 Mean Climate**

135 Since about 75% of the global surface is ocean, in the simulations of the mean climate, we  
 136 expect a similar model response in our experiments by delaying  $\tau$  only over the oceans, as ear-

Experiment Name	$\tau_L$	$\tau_O$
<i>EXPT<sub>fast</sub></i>	1hr	1hr
<i>EXPT<sub>2h</sub></i>	1hr	2hr
<i>EXPT<sub>3h</sub></i>	1hr	3hr
<i>EXPT<sub>4h</sub></i>	1hr	4hr
<i>EXPT<sub>slow</sub></i>	4hr	4hr

**Table 1.**  $\tau$  values for different experiments

132

137 lier studies did by having a larger  $\tau$  globally. An evaluation of some of the mean features of sim-  
 138 ulated climate in our experiments confirm this. We find an increase in large-scale rainfall and a  
 139 decrease in convective rain going from *EXPT<sub>fast</sub>* to *EXPT<sub>slow</sub>* (Fig 1 and Supplementary Fig  
 140 S1). Similarly, we also notice warming in the lower levels, stronger warming in the upper lev-  
 141 els, slight cooling in the mid-levels; moistening in the lower levels, and drying in the mid-levels  
 142 (Fig 2 and Supplementary Fig S2). These features have been reported in earlier studies [for ex-  
 143 ample, Fig 8 in *Mishra and Srinivasan, 2010*].

144 Investigating the mean features for land and ocean separately, we notice in addition, lower  
 145 level (upper level) warming (cooling) is more (less) over land than over oceans (Fig 2). In the case  
 146 of moisture, the letter "S" patterned vertical structure over the ocean is more curvy and squeezed  
 147 down meaning lower level (middle level) moistening (drying) is stronger over oceans than over  
 148 land and the respective peaks are vertically closer to the sea surface. These profiles, all together,  
 149 indicate a model response to changes in  $\tau$  in terms of the distribution of atmospheric convection  
 150 and clouds, which impacts heating/cooling and moistening/drying of the air column (Supplemen-  
 151 tary Fig S2). Essentially these responses indicate an accumulation of convective instability in the  
 152 atmosphere with delaying of convective adjustment time scale. It is attributable to more low-level  
 153 warming over the continents and more low-level moistening over the oceans. More moistening  
 154 near the ocean surface is relatively straightforwardly understandable, and it is a consequence of  
 155 the atmosphere taking longer to convect with larger  $\tau$ . To a zero-order approximation, as a re-  
 156 sult of the near-surface moisture pile-up in the oceanic regions, there is a moisture deficit in the  
 157 lower levels over the continental regions (Fig 3 and Supplementary Fig S3a and S3b). Indeed it  
 158 is apparent, in relative sense, in Fig 3. Although  $q_O$  does not exhibit a clear moistening signal,

159 the land drying in  $q_L$  is profound. The consequences are reflected in terms of changes in cloud  
 160 cover. In an overall declining tendency of cloud cover, from  $EXPT_{fast}$  to  $EXPT_{slow}$ , over the  
 161 tropics high clouds decrease more steeply than low clouds. Low clouds decrease less rapidly over  
 162 the ocean compared to those over land (Fig 4). It should be noted that cloud categories are ob-  
 163 jectively defined in CESM. For example, low-level clouds are the ones below 700 hPa and high  
 164 clouds are between 400 and 50 hPa. Cloud covers are integrated for each model level correspond-  
 165 ing to respective cloud categories. In that regard, going from  $EXPT_{fast}$  to  $EXPT_{slow}$ , low-cloud  
 166 cover changes (Fig 4) are consistent with relative surface moistness over land and ocean (Fig 3).

167 Taken together, the altered vertical profiles of moisture and temperature, distribution of con-  
 168 vective and large-scale rainfall, and associated clouds are consistent with the idea that convec-  
 169 tion is short-lived and stronger for smaller  $\tau$  values and long-lived and weaker for longer  $\tau$  value.  
 170 It is also evident from the solution of the CAPE equation in the ZM scheme, which can be ex-  
 171 pressed as  $CAPE(t) = CAPE_o \exp(-\frac{t}{\tau})$  in the absence of large-scale CAPE generation, where  
 172  $CAPE_o$  is the values of CAPE at  $t = 0$ . A larger  $\tau$  in this expression means a slower decay of  
 173 CAPE. The duration of convection is essentially linked with its persistence and hence "mem-  
 174 ory". We discuss its impact on the simulation of the equatorial waves in the following section.

### 175 3.2 Simulation of MJO variance and propagation

176 Organization is a primary feature of tropical convection. It essentially means a cluster of  
 177 deep precipitating clouds tied together. An important question is, what brings these clouds to-  
 178 gether? In other words, what causes convection to organize? One idea to see the organization of  
 179 convection is through superpositions of convectively coupled equatorial waves (CCEWs). These  
 180 atmospheric waves and tropical convection are entangled. In the tropics, the atmosphere responds  
 181 to convective heating in terms of waves that, in turn, organize convection. Therefore, the fidelity  
 182 of a model in simulating tropical climate is essentially its ability to simulate the CCEWs. A stan-  
 183 dard metric to analyze CCEWs is the Takayabu-Wheeler-Kiladis (TWK) spectra [*Takayabu, 1994a,b;*  
 184 *Wheeler and Kiladis, 1999*]. Figure 5 depicts the symmetric and asymmetric TWK-spectra for  
 185 the observed and simulated outgoing long-wave radiation (OLR). Understandably, a striking fea-  
 186 ture of the TWK-spectra of observed OLR shown in Fig 5a and b is the spectral power near the  
 187 origin of the plots in the wavenumber range 1-5 and frequency 20-100 days, well known as the  
 188 MJO. The MJO is a combination of or envelope of other waves in the equatorial atmosphere. Hence,  
 189 the accuracy of MJO simulation is arguably a measure of the fidelity of accurate simulation of

190 waves in the atmosphere [Zhang *et al.*, 2020]. Guo *et al.* [2015] showed in detail that the accu-  
 191 racy of CCEW simulation is critical for a realistic MJO simulation.

192 A comprehensive review of the science of MJO is available in Zhang *et al.* [2020]. Promi-  
 193 nent observed features of MJO suggest that they are most active in the Indo-Pacific warm pool  
 194 with an eastward propagation. An interesting fact, along its path from the Indian to the Pacific  
 195 Ocean, is that an MJO passes over the Indonesian maritime continent (IMC). During this pas-  
 196 sage, MJO and the prominent diurnal variabilities in the meteorology over the IMC islands in-  
 197 teract and mutually influence each other. So much so that nearly half of the MJOs fail to prop-  
 198 agate into the Pacific. It is critical, therefore, to represent the land-ocean heterogeneity as real-  
 199 istically as possible in climate models. Hence, we expect our experiments with logically defined  
 200 different values of  $\tau$  for land and ocean to improve simulated MJO features. Here, we shall present  
 201 analyses evaluating the simulation of MJO variance and propagation. We can draw some idea  
 202 of MJO simulation in different experiments from Fig 5. In Fig 5, the foremost remarkable fea-  
 203 ture is the increase in spectral power in the MJO wave number and frequency range for experi-  
 204 ments with a longer  $\tau$ . A closer visual inspection reveals that the MJO spectral power does not  
 205 dramatically change from  $EXPT_{2h}$  to  $EXPT_{slow}$ . For other waves, no one simulation is remark-  
 206 ably better than the rest. Fig 5 loosely suggests that overall the symmetric signal waves are im-  
 207 proved for longer time scales, but there are no clear improvement for the antisymmetric part.

208 To bring out the active region of MJO we applied space-time filtering on OLR data con-  
 209 taining the signal corresponding to wavenumbers 1-5 and a period of 20–100 days. In Fig 6 the  
 210 variance of the MJO-filtered daily OLR anomalies is shown. In observations (Fig 6a), the peak  
 211 variance is over the Indo-Pacific warm pool. Feeble variance peaks are noted in the eastern sides  
 212 of the Pacific (off the Gulf of California) and Atlantic (around the western coast of Sierra Leone).  
 213 It is consistent with the fact that although MJO is most active in the Indo-Pacific warm pool re-  
 214 gion, it has considerable influence modulating the convective activity over the eastern equato-  
 215 rial Pacific [Maloney and Hartmann, 2000a,b; Maloney and Kiehl, 2002] and Atlantic [Klotzbach,  
 216 2014]. For  $EXPT_{fast}$  high variance is noted around the warm-pool region but widely spread and  
 217 has multiple peaks. The strongest variance is around Northern Australia and the south-western  
 218 Pacific region. The other secondary maxima are over the southern Bay of Bengal, the central equa-  
 219 torial Indian Ocean, and the central Pacific regions.

220 The simulated MJO variance strength and pattern experience some changes with changes  
 221 in  $\tau$  values. In general, a slower  $\tau_O$  keeping  $\tau_L$  same yields more variance. In other words, it in-

222 creases convective activity in MJO space and time scales. In  $EXPT_{2h}$  a pronounced peak is  
 223 located over the western-central equatorial Pacific with two secondary maxima near the south-western  
 224 equatorial Pacific and eastern equatorial Indian Ocean. In  $EXPT_{3h}$  the variance is more concen-  
 225 trated over the western equatorial Pacific, with a secondary peak south of the central equatorial  
 226 Indian Ocean. With larger values of  $\tau_L$ , the maximum variance gets more and more focused over  
 227 the warm pool region, from  $EXPT_{fast}$  to  $EXPT_{3h}$  (comparing Fig 6b-d). It is noteworthy, that  
 228 all the pronounced peaks for  $EXPT_{2h}$  and  $EXPT_{3h}$  are over oceans, in and around the Indo-Pacific  
 229 warm pool region, but split unlike observations (Fig 6a). The model simulated MJO variance fur-  
 230 ther slowing  $\tau_O$  to 4 hours ( $EXPT_{4h}$  shown in Fig 6e) suggests that MJO variance does not nec-  
 231 essarily increase with increasing  $\tau_O$ . The variance peak intensities are visibly weaker in  $EXPT_{04}$   
 232 compared to that in  $EXPT_{2h}$  and  $EXPT_{3h}$  and more only than that in  $EXPT_{fast}$ . However, a note-  
 233 worthy feature of  $EXPT_{4h}$ , a fine detail missing in all other simulations, is the variance peaks  
 234 near the eastern side of the equatorial Pacific and Atlantic oceans. Baring these subtle variance  
 235 peaks,  $EXPT_{slow}$  looks the best, although still a considerably weaker variance peak compared  
 236 to observations. The variance fields normalized by the respective domain means are available  
 237 in Supplementary Fig S4, which depicts a better visual illustration of the variance peaks.

238 A prominent feature of MJOs is eastward propagation. The propagation features of the MJO  
 239 are arguably better characterized by Hovmöller plots averaged over the latitude band between 10°S  
 240 and 10°N, shown in Fig 7. Each frame in Fig 7 depicts 10°S-10°N averaged cross-correlations  
 241 of OLR anomalies with MJO-index. The MJO-index is defined as the 20-100-day filtered OLR  
 242 anomalies averaged over 5°S-5°N, 75°E-85°E following *Guo et al. [2015]*. It is noteworthy to  
 243 mention, reiterating *Guo et al. [2015]*, the philosophy behind using such an MJO index. An in-  
 244 dex based on a 20-100 day filter brings out the dominant intraseasonal signal in the data that ide-  
 245 ally should be an MJO signal. The eastward propagating red and blue patches of correlation val-  
 246 ues in observations (Fig 7a) confirm it. We note the phase speed is faster over the west Pacific  
 247 (east of ~120°E) than that over the Indian Ocean (west of ~100°E). The relatively slow phase speed  
 248 in the longitude range ~100°-120°E is collocated with the Indonesian archipelago. These dif-  
 249 ferent phase speeds over land and oceanic regions are consistent with MJO interaction with the  
 250 profound diurnal variations of meteorology over the MC. It furthermore emphasizes the need to  
 251 mimic land-ocean heterogeneity realistically in climate models.

252 To assess the performance of our different experiments in simulating MJO propagation fea-  
 253 tures, we recall the "good" and "bad" models of *Guo et al. [2015]*. In Figure 2, *Guo et al. [2015]*  
 254 showed that the "good" models simulated more realistic eastward propagation than the "bad" mod-

255 els. In Fig 7,  $EXPT_{4h}$  is the only experiment with an eastward propagation and exhibits some  
 256 resemblance with observations and the only "good" model, albeit with some key caveats. The  
 257 positive anomalies almost abruptly died over the MC and reappeared over the western Pacific.  
 258 Nonetheless, an intriguing observation, that contains the novelty of our research, is the more re-  
 259 alistic eastward propagation simulated in  $EXPT_{4h}$  than in  $EXPT_{slow}$ . An improved simulation  
 260 of eastward propagation in  $EXPT_{4h}$  supports our argument that using two  $\tau$ s for land and ocean  
 261 is a logical choice. It reconfirms our anticipation that representing land-ocean heterogeneity via  
 262  $\tau$  in ZM in CAM alters convective memory and affects the organization of convection. A larger  
 263  $\tau_O$  than  $\tau_L$ , although reasonable, is only based on intuition. Detailed sensitivity analysis would  
 264 be needed to investigate and pin down the best pair of  $\tau$  values.

#### 265 **4 Discussion and Conclusion**

266 Climate models continue to grow, fueled by a growing understanding of the earth system.  
 267 Hence, it is only logical to include a fairly well-recognized and relatively old knowledge about  
 268 land and ocean heterogeneity of atmospheric convection in the parameterization of convection.  
 269 We argue that using two different  $\tau$  in ZM in CAM can be one simple yet fruit-bearing way. In  
 270 our experiments to investigate the model response to land-ocean heterogeneity in  $\tau$  values, we  
 271 used  $\tau_L = 1$  hr, and  $\tau_O = 2$  hrs, 3 hrs, 4 hrs. In two additional experiments,  $EXPT_{fast}$  and  $EXPT_{slow}$ ,  
 272 we used  $\tau_L = \tau_O = 1$  hr and  $\tau_L = \tau_O = 4$  hrs, respectively, to complement the previous group  
 273 of experiments. The  $\tau$  values that we have used are informed by our knowledge of frequency, life-  
 274 cycle, and behavior of atmospheric convection over land and ocean learned from previous stud-  
 275 ies [Lucas *et al.*, 1994; Williams and Stanfill, 2002; Zipser *et al.*, 2006; Hagos *et al.*, 2013; Mat-  
 276 sui *et al.*, 2016; Roca *et al.*, 2017; Roca and Fiolleau, 2020] and inspired by results of relevant  
 277 model sensitivity experiments [Zhang and McFarlane, 1995; Lee *et al.*, 2009; Mishra and Srini-  
 278 vasan, 2010; Mishra, 2011; Misra *et al.*, 2012].

279 Our findings regarding the model simulated mean state in different experiments are con-  
 280 sistent with earlier studies [Lee *et al.*, 2009; Mishra and Srinivasan, 2010; Mishra, 2011; Misra  
 281 *et al.*, 2012]. For example, total rainfall remained approximately the same while large-scale rain-  
 282 fall increased and convective rain decreased for longer  $\tau_L$ s. Consistency of the model response  
 283 for a slow  $\tau$  only over the oceans with slowing down  $\tau$  globally is most likely a result of 75% of  
 284 the global surface being ocean. However, since there is no physical barrier between the atmospheric  
 285 columns over continents and oceans, having two  $\tau$  values in our experiments, which essentially  
 286 are prescribed to represent heterogeneity in the persistence of convection over the two different

287 surfaces, created a distinction between the intensities with which the model responses are felt over  
288 land and ocean. For example, the oceanic boundary layer is moister and warmer than the con-  
289 tinental boundary layer (Fig 3). Furthermore, the mid-troposphere is drier and cooler over oceans  
290 than over the continents (Fig 2). These land-ocean heterogeneities inevitably create differences  
291 in atmospheric instabilities. These instabilities are essentially realized in the form of atmospheric  
292 convection that, by design in our experiments with slower  $\tau$ , takes longer to bring the atmosphere  
293 back to a background state. It is suggestive of a longer persistence of convective instability over  
294 the ocean than that over the continents which essentially can be linked with memory of convec-  
295 tion [Davies *et al.*, 2009; Colin *et al.*, 2019; Hwong *et al.*, 2023].

296 The conclusion that the model simulated better convectively coupled equatorial waves in  
297  $EXPT_{2h}$  than in  $EXPT_{slow}$  is a key. We conclude this based on our finding of a better MJO sim-  
298 ulation in  $EXPT_{2h}$ , consistent with improved symmetric waves. Scientists had advocated in fa-  
299 vor of a slower  $\tau$  in earlier studies [Mishra, 2011; Misra *et al.*, 2012]. We also noted a signifi-  
300 cant increase in MJO power for  $\tau = 4$  hrs than  $\tau = 1$  hr (comparing Fig 5b and Fig 5f). However,  
301 an evaluation of the model simulated intraseasonal zonal propagation reveals that  $EXPT_{4h}$  per-  
302 forms considerably better than  $EXPT_{slow}$ . This confirms that having one  $\tau$  globally is not only  
303 unphysical but also slowing down tinkering persistence of convection to improve simulation of  
304 equatorial waves, and may result in model responses that might look improved, but only super-  
305 ficially.

306 Our results, in general, serve as proof of concept that a realistic representation of convec-  
307 tive adjustment time scale over land and ocean is a logical requirement that properly implemented  
308 shall lead to improvements in climate model simulations. In specific, we advocate at least two  
309  $\tau$  values, one for the continents and one relatively slower for the oceans in ZM in CAM. The fact  
310 that we did not perform a rigorous model sensitivity analysis [e.g., Qian *et al.*, 2015; Lin *et al.*,  
311 2016; Goswami *et al.*, 2017] nor did we perform any cloud-resolving simulation targeting the  
312 life-cycle of atmospheric convection [Davies *et al.*, 2013; Colin *et al.*, 2019; Daleu *et al.*, 2020,  
313 e.g.,] leaves a scope as well as the requirement for future research to determine the best values  
314 of  $\tau_L$  and  $\tau_O$  for ZM in CAM. It will hopefully guide convection parameterization schemes, es-  
315 pecially the adjustment types, to address land-ocean heterogeneity. Specifically, we recommend  
316 that future developments of CAM should consider prescribing different  $\tau_L$  and  $\tau_O$  in ZM in CAM.

## 5 Open Research

- 318 • Model : We used the atmospheric model of the Community Earth System Model, version  
319 2.1.3 (CESM 2.1.3) [Danabasoglu *et al.*, 2020]
- 320 • Description of the model simulations is provided in Section 2 of the manuscript. A source  
321 file of CESM 2.1.3, zm\_conv.F90, modified for our experiments is provided in [https://github.com/bidyutbg/CESM\\_Tau\\_experiment.git](https://github.com/bidyutbg/CESM_Tau_experiment.git).  
322
- 323 • Data analysis software: Figures 1-5 are produced in Python and the details of the method-  
324 ology is provided in the relevant sections of the text. Figure 5 is produced using script avail-  
325 able at [https://github.com/bidyutbg/CESM\\_Tau\\_experiment/blob/main/WK\\_spectra\\_FINAL-NEW.ipynb](https://github.com/bidyutbg/CESM_Tau_experiment/blob/main/WK_spectra_FINAL-NEW.ipynb). Figure 6 is produced using script available at [https://github.com/bidyutbg/CESM\\_Tau\\_experiment/blob/main/CCEW\\_variance-compare\\_FINAL.ipynb](https://github.com/bidyutbg/CESM_Tau_experiment/blob/main/CCEW_variance-compare_FINAL.ipynb). Figure 7 is produced using script available at [https://www.ncl.ucar.edu/Applications/Scripts/mjoclivar\\_9.ncl](https://www.ncl.ucar.edu/Applications/Scripts/mjoclivar_9.ncl).  
326  
327  
328  
329
- 330 • Model Output Data: Data archival is underway in Zenodo. Archival will be completed  
331 soon. A sample of the data is provided as Supporting Information for review purposes.

## Acknowledgments

332 The authors gratefully acknowledge funding from the European Research Council (ERC) under  
333 the European Union’s Horizon 2020 research and innovation program (Project CLUSTER, Grant  
334 Agreement No. 805041). This research was supported by the Scientific Service Units (SSU) of  
335 ISTA through resources provided by Scientific Computing (SciComp).  
336

## References

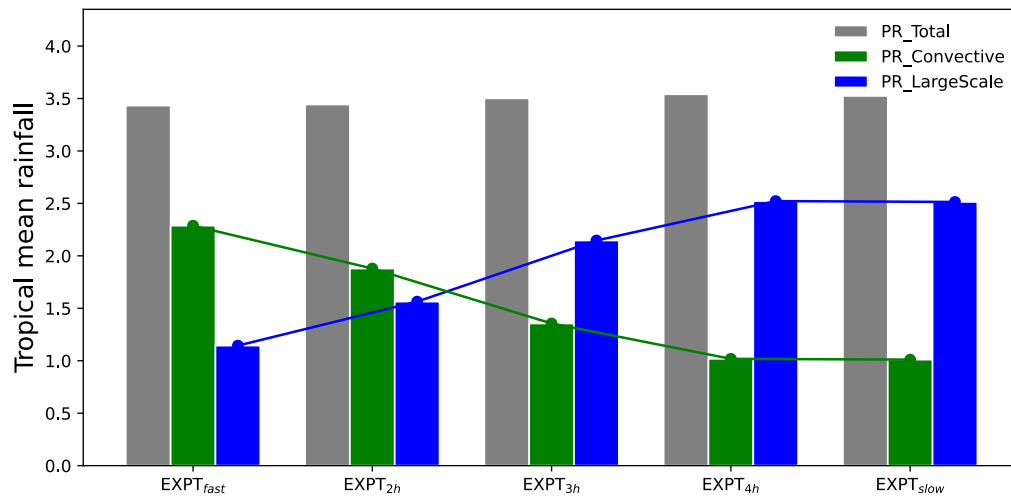
- 337
- 338 Arakawa, A. (2004), The Cumulus Parameterization Problem: Past, Present, and Future,  
339 *Journal of Climate*, 17(13), 2493–2525, doi:10.1175/1520-0442(2004)017<2493:  
340 RATCPP>2.0.CO;2.
- 341 Colin, M., S. Sherwood, O. Geoffroy, S. Bony, and D. Fuchs (2019), Identifying the Sources  
342 of Convective Memory in Cloud-Resolving Simulations, *Journal of the Atmospheric  
343 Sciences*, 76(3), 947–962, doi:10.1175/JAS-D-18-0036.1.
- 344 Daleu, C. L., R. S. Plant, S. J. Woolnough, A. J. Stirling, and N. J. Harvey (2020), Memory  
345 Properties in Cloud-Resolving Simulations of the Diurnal Cycle of Deep Convection,  
346 *Journal of Advances in Modeling Earth Systems*, 12(8), doi:10.1029/2019MS001897.

- 347 Danabasoglu, G., J. Lamarque, J. Bacmeister, D. A. Bailey, A. K. DuVivier, J. Edwards,  
348 L. K. Emmons, J. Fasullo, R. Garcia, A. Gettelman, C. Hannay, M. M. Holland, W. G.  
349 Large, P. H. Lauritzen, D. M. Lawrence, J. T. M. Lenaerts, K. Lindsay, W. H. Lipscomb,  
350 M. J. Mills, R. Neale, K. W. Oleson, B. Otto-Bliesner, A. S. Phillips, W. Sacks, S. Tilmes,  
351 L. Kampenhout, M. Vertenstein, A. Bertini, J. Dennis, C. Deser, C. Fischer, B. Fox-  
352 Kemper, J. E. Kay, D. Kinnison, P. J. Kushner, V. E. Larson, M. C. Long, S. Mickelson,  
353 J. K. Moore, E. Nienhouse, L. Polvani, P. J. Rasch, and W. G. Strand (2020), The Com-  
354 munity Earth System Model Version 2 (CESM2), *Journal of Advances in Modeling Earth*  
355 *Systems*, 12(2), doi:10.1029/2019MS001916.
- 356 Davies, L. (2008), Self-organisation of convection as a mechanism for memory, Ph.D. thesis,  
357 The University of Reading.
- 358 Davies, L., R. S. Plant, and S. H. Derbyshire (2009), A simple model of convection with  
359 memory, *Journal of Geophysical Research: Atmospheres*, 114(D17), 17,202, doi:  
360 10.1029/2008JD011653.
- 361 Davies, L., R. S. Plant, and S. H. Derbyshire (2013), Departures from convective equilibrium  
362 with a rapidly varying surface forcing, *Quarterly Journal of the Royal Meteorological*  
363 *Society*, 139(676), 1731–1746, doi:10.1002/qj.2065.
- 364 Goswami, B. B., B. Khouider, R. Phani, P. Mukhopadhyay, and A. J. Majda (2017),  
365 Implementation and calibration of a stochastic multcloud convective parameteriza-  
366 tion in the NCEP <sc>C</sc> limate <sc>F</sc> orecast <sc>S</sc> ystem  
367 (CFSv2), *Journal of Advances in Modeling Earth Systems*, 9(3), 1721–1739, doi:  
368 10.1002/2017MS001014.10.1002/2017MS001014.
- 369 Guo, Y., D. E. Waliser, and X. Jiang (2015), A Systematic Relationship between the Rep-  
370 resentations of Convectively Coupled Equatorial Wave Activity and the Madden–Julian  
371 Oscillation in Climate Model Simulations, *Journal of Climate*, 28(5), 1881–1904, doi:  
372 10.1175/JCLI-D-14-00485.1.10.1175/JCLI-D-14-00485.1.
- 373 Hagos, S., Z. Feng, S. Mcfarlane, and L. R. Leung (2013), Environment and the Lifetime of  
374 Tropical Deep Convection in a Cloud-Permitting Regional Model Simulation, *Journal of*  
375 *the Atmospheric Sciences*, 70(8), 2409–2425, doi:10.1175/JAS-D-12-0260.1.
- 376 Hourdin, F., T. Mauritsen, A. Gettelman, J. C. Golaz, V. Balaji, Q. Duan, D. Folini, D. Ji,  
377 D. Klocke, Y. Qian, F. Rauser, C. Rio, L. Tomassini, M. Watanabe, and D. Williamson  
378 (2017), The Art and Science of Climate Model Tuning, *Bulletin of the American Meteorolo-*  
379 *logical Society*, 98(3), 589–602, doi:10.1175/BAMS-D-15-00135.1.

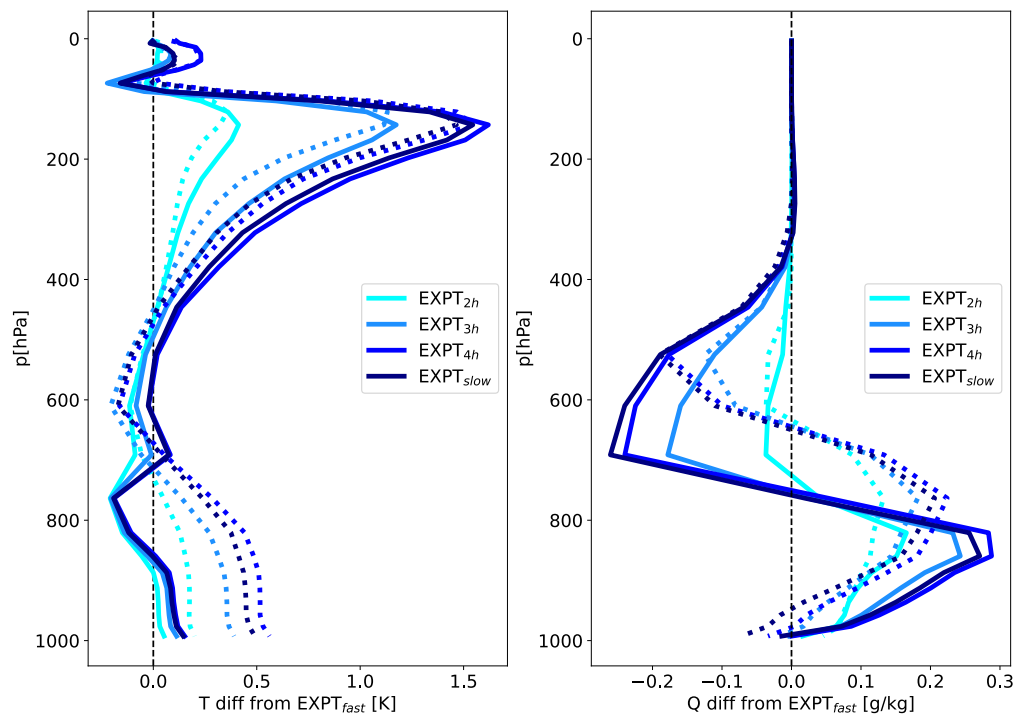
- 380 Hwong, Y.-L., M. Colin, P. Aglas-Leitner, C. Muller, and S. Sherwood (2023), Assessing  
381 Memory in Convection Schemes Using Idealized Tests, *ESS Open Archive*, preprint.
- 382 Klotzbach, P. J. (2014), The Madden–Julian Oscillation’s Impacts on Worldwide Tropical  
383 Cyclone Activity, *Journal of Climate*, 27(6), 2317–2330, doi:10.1175/JCLI-D-13-00483.  
384 1.
- 385 Lee, J. E., R. Pierrehumbert, A. Swann, and B. R. Lintner (2009), Sensitivity of stable water  
386 isotopic values to convective parameterization schemes, *Geophysical Research Letters*,  
387 36(23), doi:10.1029/2009GL040880.
- 388 Liebmann, B., and C. Smith (1996), Description of a Complete (Interpolated) Outgoing  
389 Longwave Radiation Dataset., *Bulletin of the American Meteorological Society*, 77, 1275–  
390 1277.
- 391 Lin, G., H. Wan, K. Zhang, Y. Qian, and S. J. Ghan (2016), Can nudging be used to quantify  
392 model sensitivities in precipitation and cloud forcing?, *Journal of Advances in Modeling  
393 Earth Systems*, 8(3), 1073–1091, doi:10.1002/2016MS000659.
- 394 Lucas, C., E. J. Zipser, and M. A. Lemone (1994), Vertical Velocity in Oceanic Convec-  
395 tion off Tropical Australia, *Journal of the Atmospheric Sciences*, 51(21), 3183–3193,  
396 doi:10.1175/1520-0469(1994)051<3183:VVIOCO>2.0.CO;2.
- 397 Maloney, E. D., and D. L. Hartmann (2000a), Modulation of Eastern North Pacific Hur-  
398 ricanes by the Madden–Julian Oscillation, *Journal of Climate*, 13(9), 1451–1460, doi:  
399 10.1175/1520-0442(2000)013<1451:MOENPH>2.0.CO;2.
- 400 Maloney, E. D., and D. L. Hartmann (2000b), Modulation of Hurricane Activity in the  
401 Gulf of Mexico by the Madden-Julian Oscillation, *Science*, 287(5460), 2002–2004, doi:  
402 10.1126/science.287.5460.2002.
- 403 Maloney, E. D., and J. T. Kiehl (2002), MJO-Related SST Variations over the Tropical East-  
404 ern Pacific during Northern Hemisphere Summer, *Journal of Climate*, 15(6), 675–689,  
405 doi:10.1175/1520-0442(2002)015<0675:MRSVOT>2.0.CO;2.
- 406 Matsui, T., J. D. Chern, W. K. Tao, S. Lang, M. Satoh, T. Hashino, and T. Kubota (2016),  
407 On the Land–Ocean Contrast of Tropical Convection and Microphysics Statistics Derived  
408 from TRMM Satellite Signals and Global Storm-Resolving Models, *Journal of Hydrome-  
409 teorology*, 17(5), 1425–1445, doi:10.1175/JHM-D-15-0111.1.
- 410 Mishra, S. K. (2011), Influence of convective adjustment time scale on the tropi-  
411 cal transient activity, *Meteorology and Atmospheric Physics*, 114(1), 17–34, doi:  
412 10.1007/S00703-011-0154-8/FIGURES/19.

- 413 Mishra, S. K. (2012), Effects of convective adjustment time scale on the simulation  
414 of tropical climate, *Theoretical and Applied Climatology*, *107*(1-2), 211–228, doi:  
415 10.1007/S00704-011-0479-8/FIGURES/19.
- 416 Mishra, S. K., and J. Srinivasan (2010), Sensitivity of the simulated precipitation to changes  
417 in convective relaxation time scale, *Annales Geophysicae*, *28*(10), 1827–1846, doi:  
418 10.5194/ANGE0-28-1827-2010.
- 419 Misra, V., P. Pantina, S. Chan, and S. DiNapoli (2012), A comparative study of the Indian  
420 summer monsoon hydroclimate and its variations in three reanalyses, *Climate Dynamics*,  
421 *39*(5), 1149–1168, doi:10.1007/s00382-012-1319-y.
- 422 Qian, Y., H. Yan, Z. Hou, G. Johannesson, S. Klein, D. Lucas, R. Neale, P. Rasch,  
423 L. Swiler, J. Tannahill, H. Wang, M. Wang, and C. Zhao (2015), Parametric sensitiv-  
424 ity analysis of precipitation at global and local scales in the Community Atmosphere  
425 Model CAM5, *Journal of Advances in Modeling Earth Systems*, *7*(2), 382–411, doi:  
426 10.1002/2014MS000354.
- 427 Randall, D., M. Khairoutdinov, A. Arakawa, and W. Grabowski (2003), Breaking the Cloud  
428 Parameterization Deadlock, *Bulletin of the American Meteorological Society*, *84*(11),  
429 1547–1564, doi:10.1175/BAMS-84-11-1547.
- 430 Randall, D. A. (2013), Beyond deadlock, *Geophysical Research Letters*, *40*(22), 5970–5976,  
431 doi:10.1002/2013GL057998.
- 432 Rayner, N. A. (2003), Global analyses of sea surface temperature, sea ice, and night ma-  
433 rine air temperature since the late nineteenth century, *Journal of Geophysical Research*,  
434 *108*(D14), doi:10.1029/2002JD002670.
- 435 Rio, C., A. D. Del Genio, and F. Hourdin (2019), Ongoing Breakthroughs in Convec-  
436 tive Parameterization, *Current Climate Change Reports 2019 5:2*, *5*(2), 95–111, doi:  
437 10.1007/S40641-019-00127-W.
- 438 Roca, R., and T. Fiolleau (2020), Extreme precipitation in the tropics is closely associated  
439 with long-lived convective systems, *Communications Earth & Environment 2020 1:1*,  
440 *1*(1), 1–6, doi:10.1038/s43247-020-00015-4.
- 441 Roca, R., T. Fiolleau, and D. Bouniol (2017), A Simple Model of the Life Cycle of  
442 Mesoscale Convective Systems Cloud Shield in the Tropics, *Journal of Climate*, *30*(11),  
443 4283–4298, doi:10.1175/JCLI-D-16-0556.1.
- 444 Stevens, B., M. Satoh, L. Auger, J. Biercamp, C. S. Bretherton, X. Chen, P. Düben, F. Judt,  
445 M. Khairoutdinov, D. Klocke, C. Kodama, L. Kornbluh, S. J. Lin, P. Neumann, W. M.

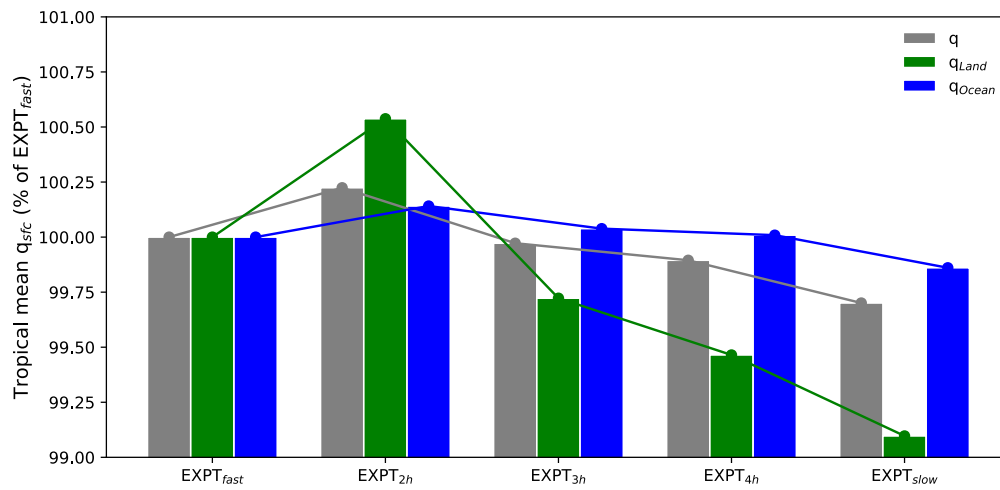
- 446 Putman, N. Röber, R. Shibuya, B. Vanniere, P. L. Vidale, N. Wedi, and L. Zhou (2019),  
447 DYAMOND: the DYnamics of the Atmospheric general circulation Modeled On  
448 Non-hydrostatic Domains, *Progress in Earth and Planetary Science*, 6(1), 1–17, doi:  
449 10.1186/S40645-019-0304-Z/FIGURES/9.
- 450 Takayabu, Y. (1994a), Large-Scale Cloud Disturbances Associated with Equatorial  
451 Waves, *Journal of the Meteorological Society of Japan. Ser. II*, 72(3), 433–449, doi:  
452 10.2151/jmsj1965.72.3{\\_}433.
- 453 Takayabu, Y. (1994b), Large-Scale Cloud Disturbances Associated with Equatorial  
454 Waves, *Journal of the Meteorological Society of Japan. Ser. II*, 72(3), 451–465, doi:  
455 10.2151/jmsj1965.72.3{\\_}451.
- 456 Wheeler, M., and G. N. Kiladis (1999), Convectively Coupled Equatorial Waves: Anal-  
457 ysis of Clouds and Temperature in the Wavenumber-Frequency Domain, *Journal of*  
458 *the Atmospheric Sciences*, 56(3), 374–399, doi:10.1175/1520-0469(1999)056<0374:  
459 CCEWAO>2.0.CO;2.
- 460 Williams, E., and S. Stanfill (2002), The physical origin of the land-ocean contrast in light-  
461 ning activity, *Comptes Rendus Physique*, 3(10), 1277–1292, doi:10.1016/S1631-0705(02)  
462 01407-X.
- 463 Zhang, C., F. Adames, B. Khouider, B. Wang, and D. Yang (2020), Four Theories of  
464 the Madden-Julian Oscillation, *Reviews of Geophysics*, 58(3), e2019RG000,685, doi:  
465 10.1029/2019RG000685.
- 466 Zhang, G. J., and N. A. McFarlane (1995), Sensitivity of climate simulations to the parame-  
467 terization of cumulus convection in the Canadian climate centre general circulation model,  
468 *Atmosphere-Ocean*, 33(3), 407–446, doi:10.1080/07055900.1995.9649539.
- 469 Zipser, E. J., D. J. Cecil, C. Liu, S. W. Nesbitt, and D. P. Yorty (2006), Where are the most:  
470 Intense thunderstorms on Earth?, *Bulletin of the American Meteorological Society*, 87(8),  
471 1057–1071, doi:10.1175/BAMS-87-8-1057.



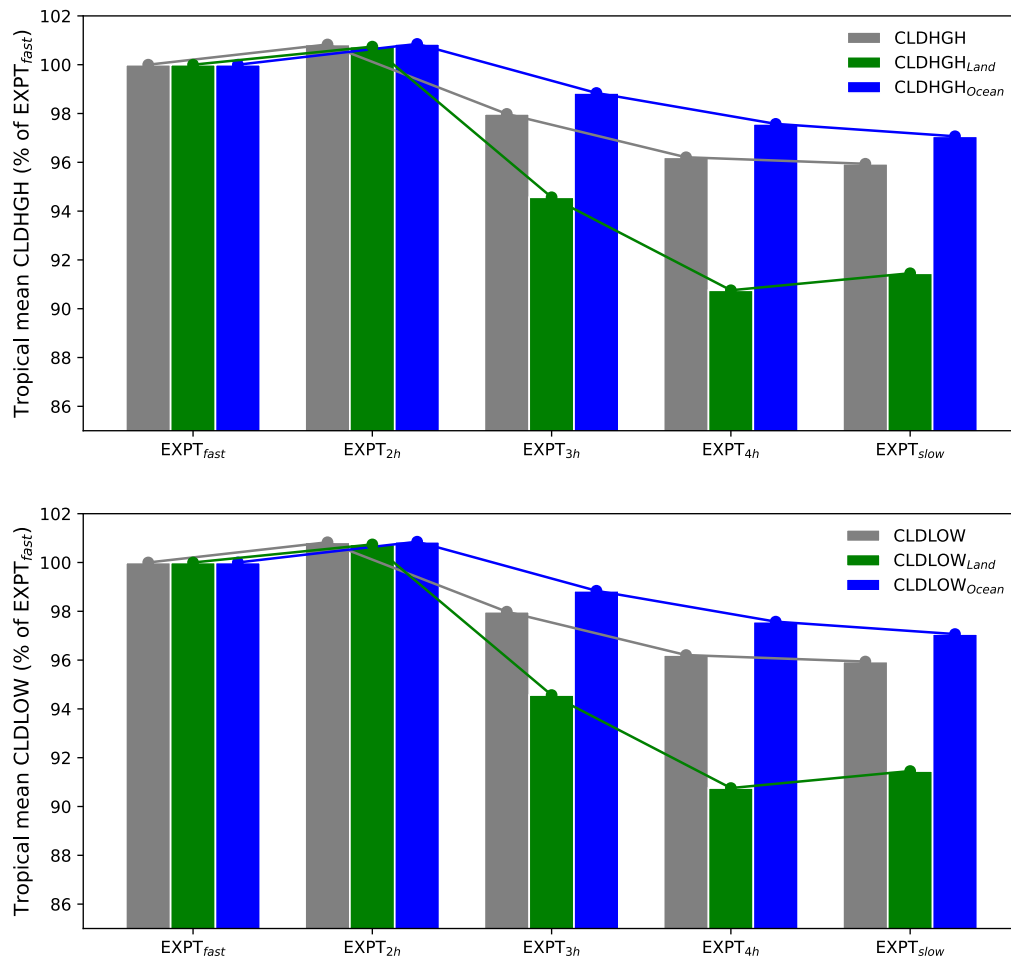
472 **Figure 1.** Tropical (tropics defined as the zonal belt between 30°S-30°N) annual mean daily rainfall  
 473 (mm/day) for different experiments mentioned in Table 1.



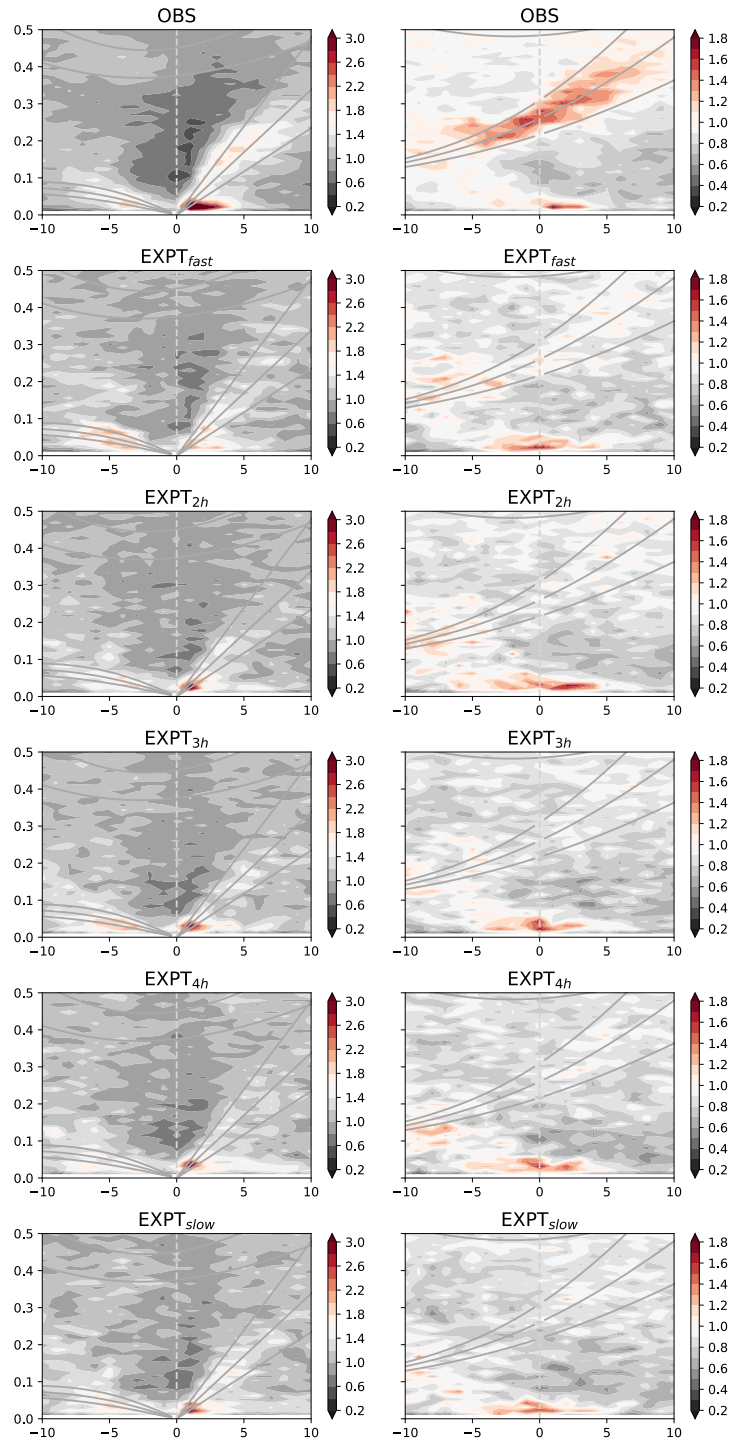
474 **Figure 2.** Tropical (tropics defined as the zonal belt between 30°S-30°N) mean vertical profiles of tem-  
 475 perature (T) and specific humidity (Q). Departures of different experiments, as indicated in the legends, from  
 476  $EXPT_{fast}$  (Land: Dotted, Ocean: Solid). The vertical dashed line indicate the zero line.



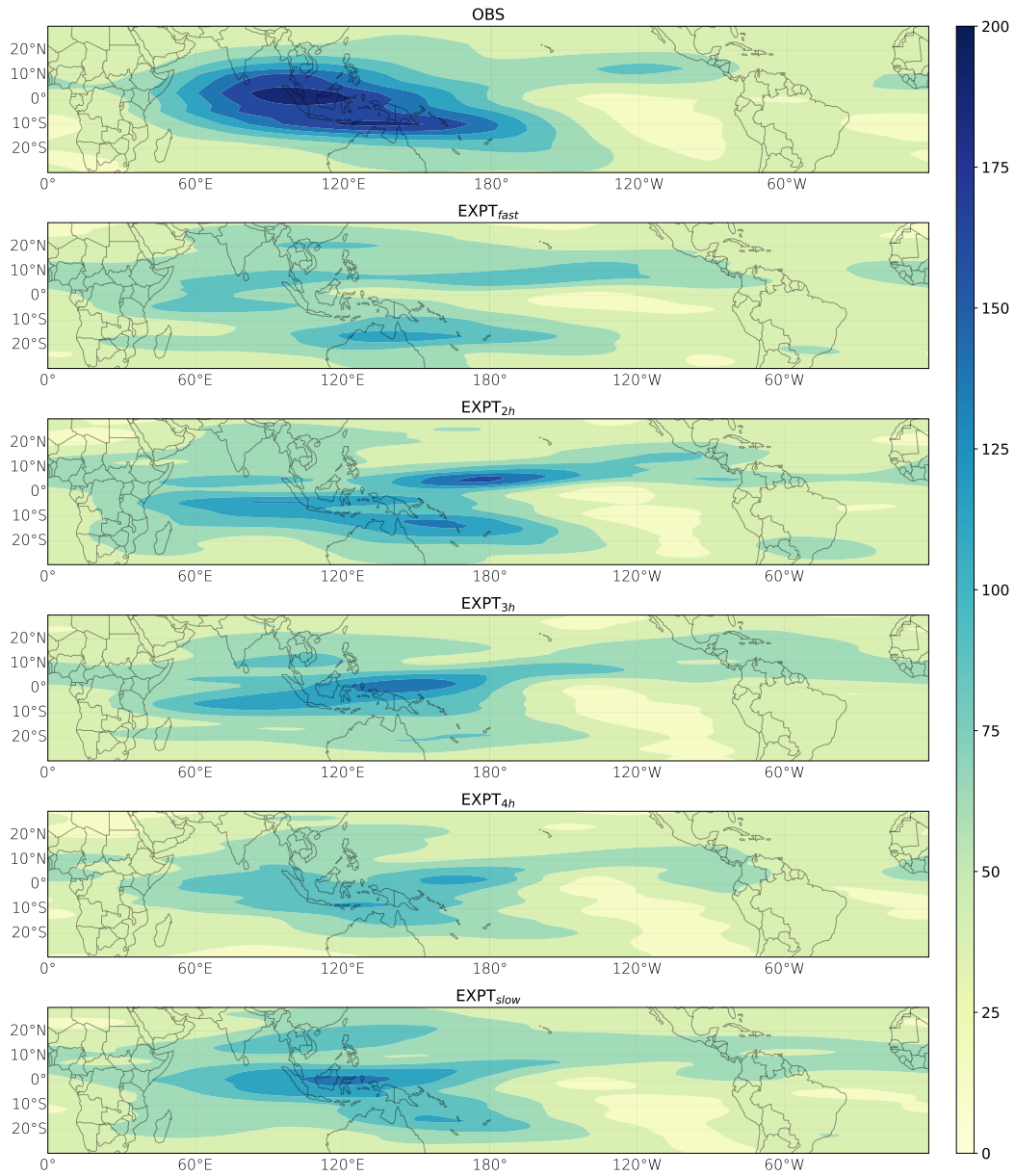
477 **Figure 3.** Tropical (tropics defined as the zonal belt between 30°S-30°N) annual daily mean specific hu-  
 478 midity as surface depicted as % of  $EXPT_{fast}$ .



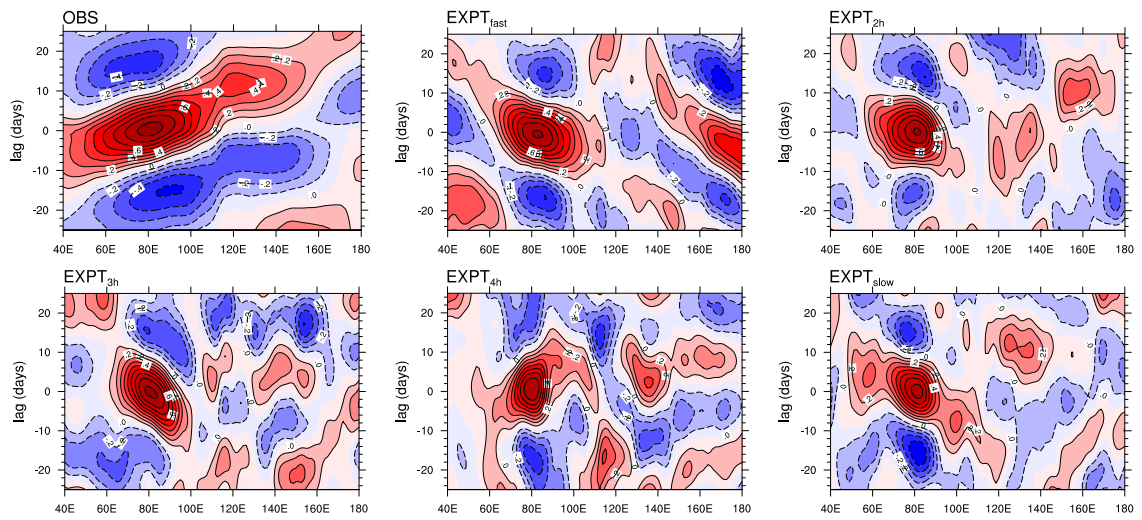
479 **Figure 4.** Tropical (tropics defined as the zonal belt between 30°S-30°N) annual daily mean High and Low  
 480 cloud cover depicted as % of  $EXPT_{fast}$ .



481 **Figure 5.** Takayabu-Wheeler-Kiladis spectra of OLR for OBS (from NOAA) and different experiments (as  
 482 named above each panel), for the symmetric component (left-hand side panels) and antisymmetric component  
 483 (right-hand side panels).



484 **Figure 6.** MJO variance computed as the daily variance of OLR data filtered for 1-5 wavenumber and 20-  
 485 100 day frequency, for OBS (from NOAA) and different experiments (as named above each panel).



486 **Figure 7.** MJO propagation: Hovmoller (averaged from 10°S to 10°N) plots of MJO-filtered OLR (W m<sup>-2</sup>)  
487 anomalies (Winter), for OBS (from NOAA) and different experiments (as named above each panel).

**Supplementary Materials for**  
An assessment of representing land-ocean  
heterogeneity via convective adjustment  
timescale in the Community Atmospheric Model  
6 (CAM6)

Bidyut Bikash Goswami,<sup>1\*</sup> Andrea Polesello,<sup>1</sup> Caroline Muller,<sup>1</sup>

<sup>1</sup>Institute of Science and Technology Austria (ISTA)  
Klosterneuburg, Austria

\*To whom correspondence should be addressed; E-mail: bgoswami@ista.ac.at

**This PDF file contains:**

- Figure S1. Annual tropical daily mean rainfall (mm/day).
- Figure S2. Tropical mean vertical profiles of DTCOND and DCQ.
- Figure S3a. Annual daily mean surface specific humidity (g/kg).
- Figure S3b. Annual daily mean mid-low-level specific humidity (g/kg).
- Figure S4. MJO variance.

Supplementary Materials

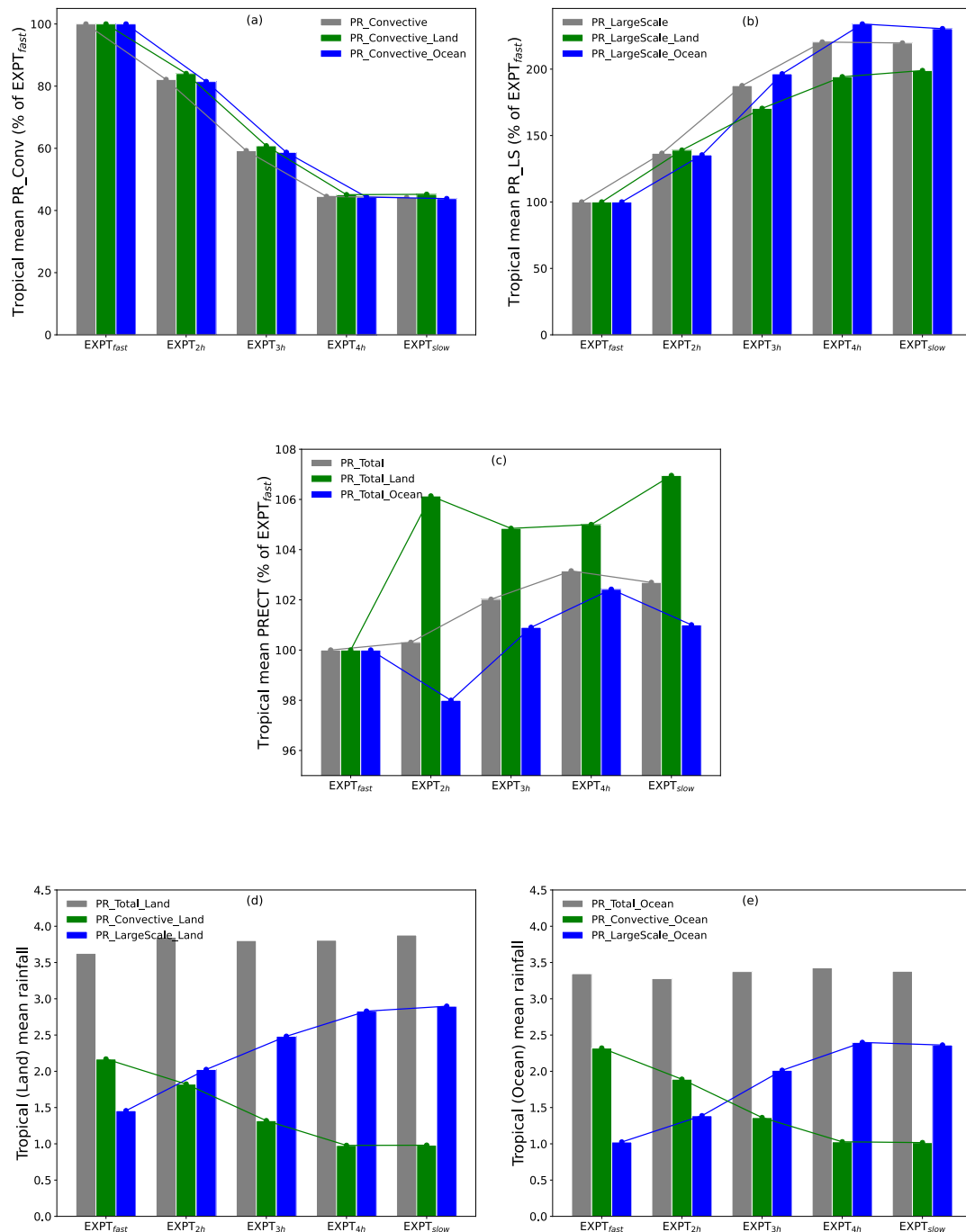


**Figure S1. Annual tropical daily mean rainfall (mm/day).** Same as Figure 1 of the main manuscript, except the Total, Convective and Large-scale rainfalls are plotted for land and ocean in addition to their total over the whole tropics.

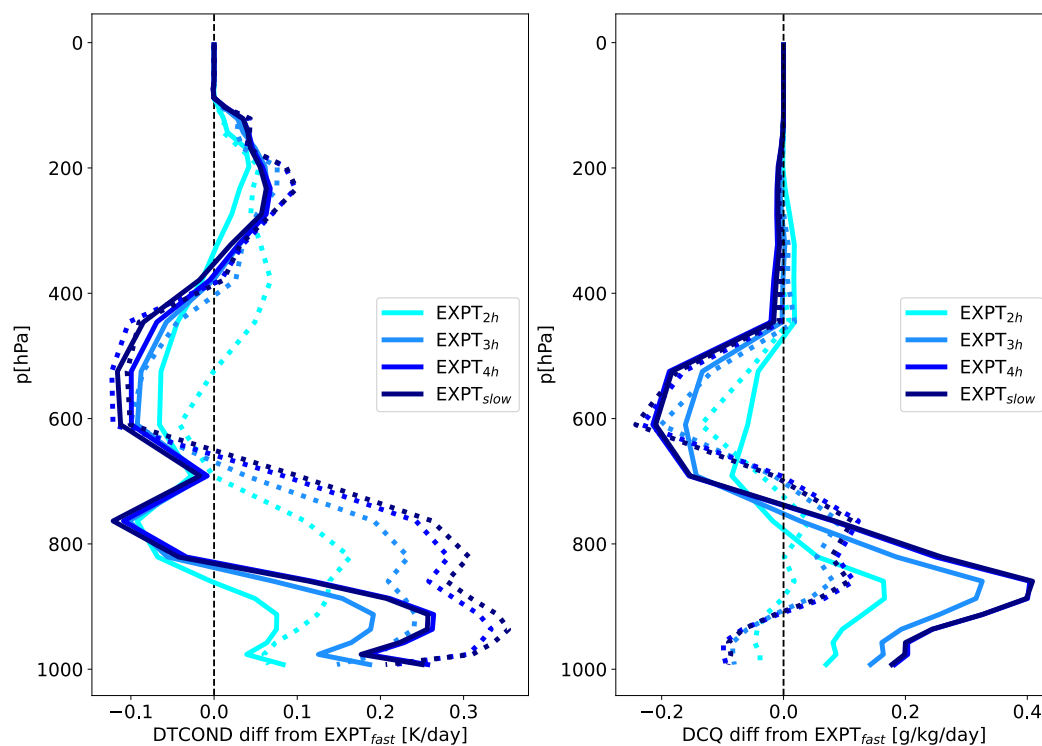


**Figure S2.** Tropical mean vertical profiles of temperature tendency due to moist processes (DTCOND) and specific humidity tendency due to moist processes (DCQ). Same as Figure 2 of the main manuscript, except for DTCOND and DCQ.

Supplementary Materials

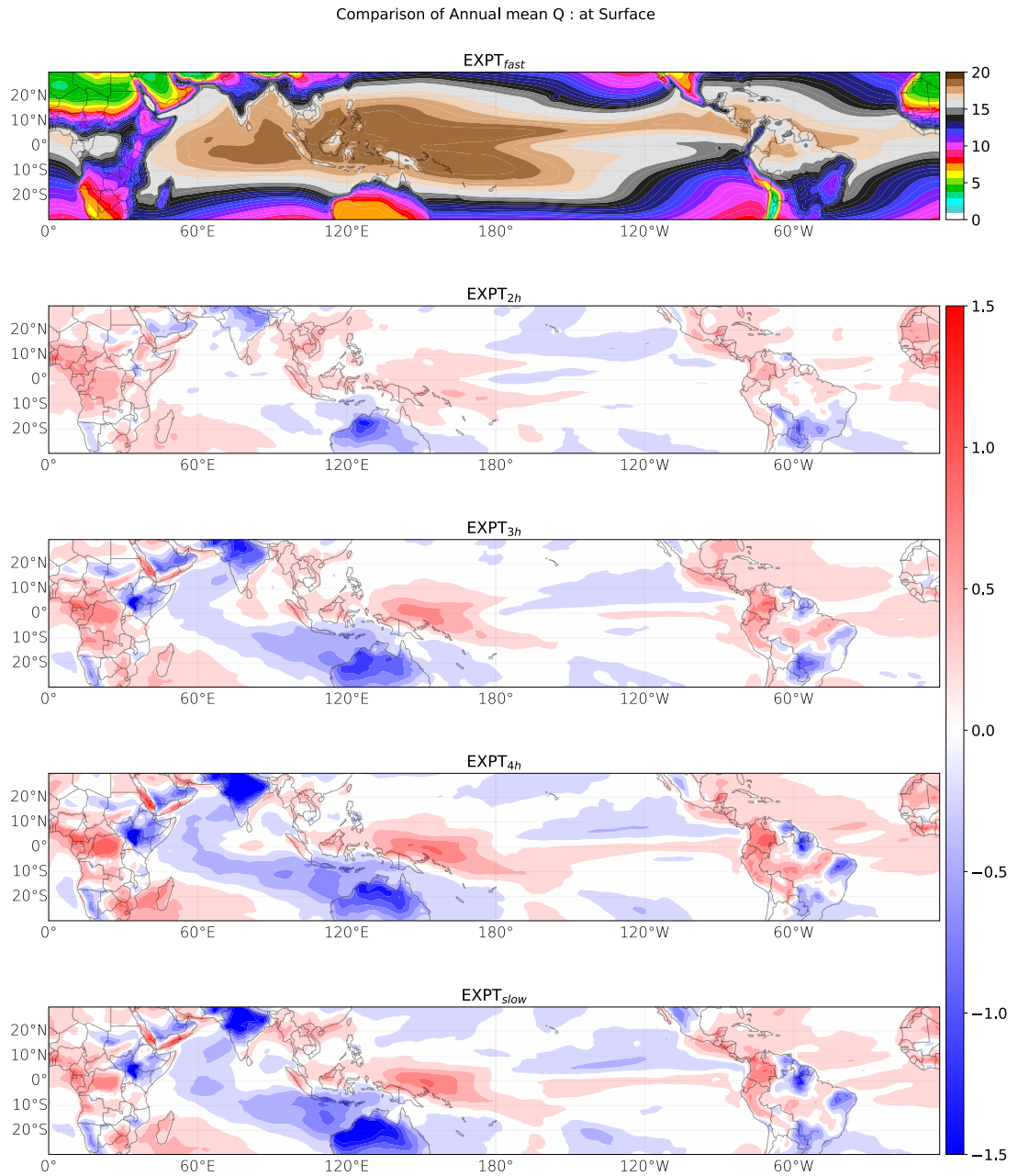


**Figure S3a. Annual daily mean surface specific humidity (g/kg).** Top panel shows the absolute values for  $EXTP_{fast}$  and the remaining panels show departures of other simulations, simulation names as indicated by the panel headings, from  $EXTP_{fast}$ .

Supplementary Materials

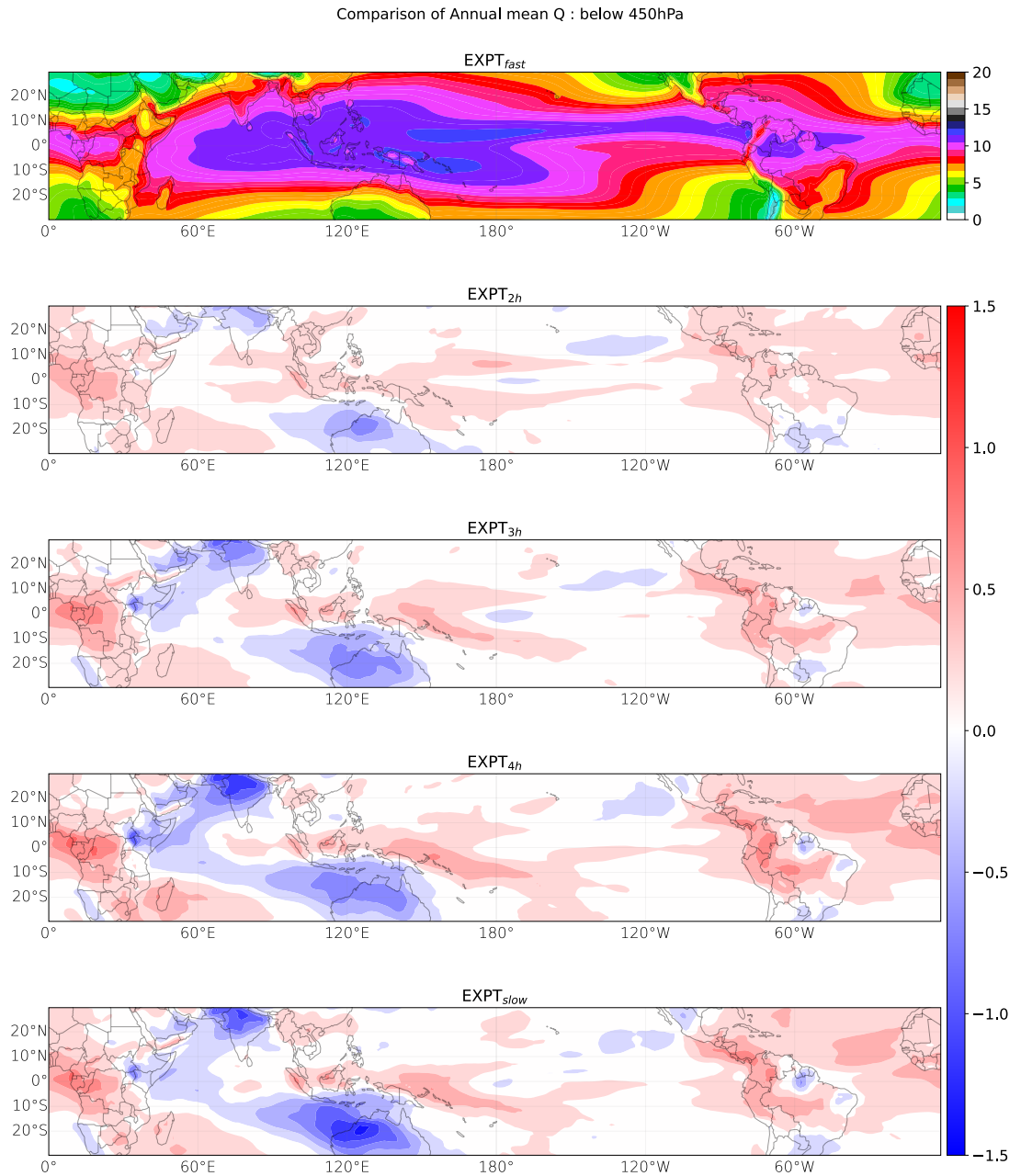


**Figure S3b.** Annual daily mean mid-low-level specific humidity (g/kg). Same as Figure S3a, except averaged over surface to 450hPa.

Supplementary Materials

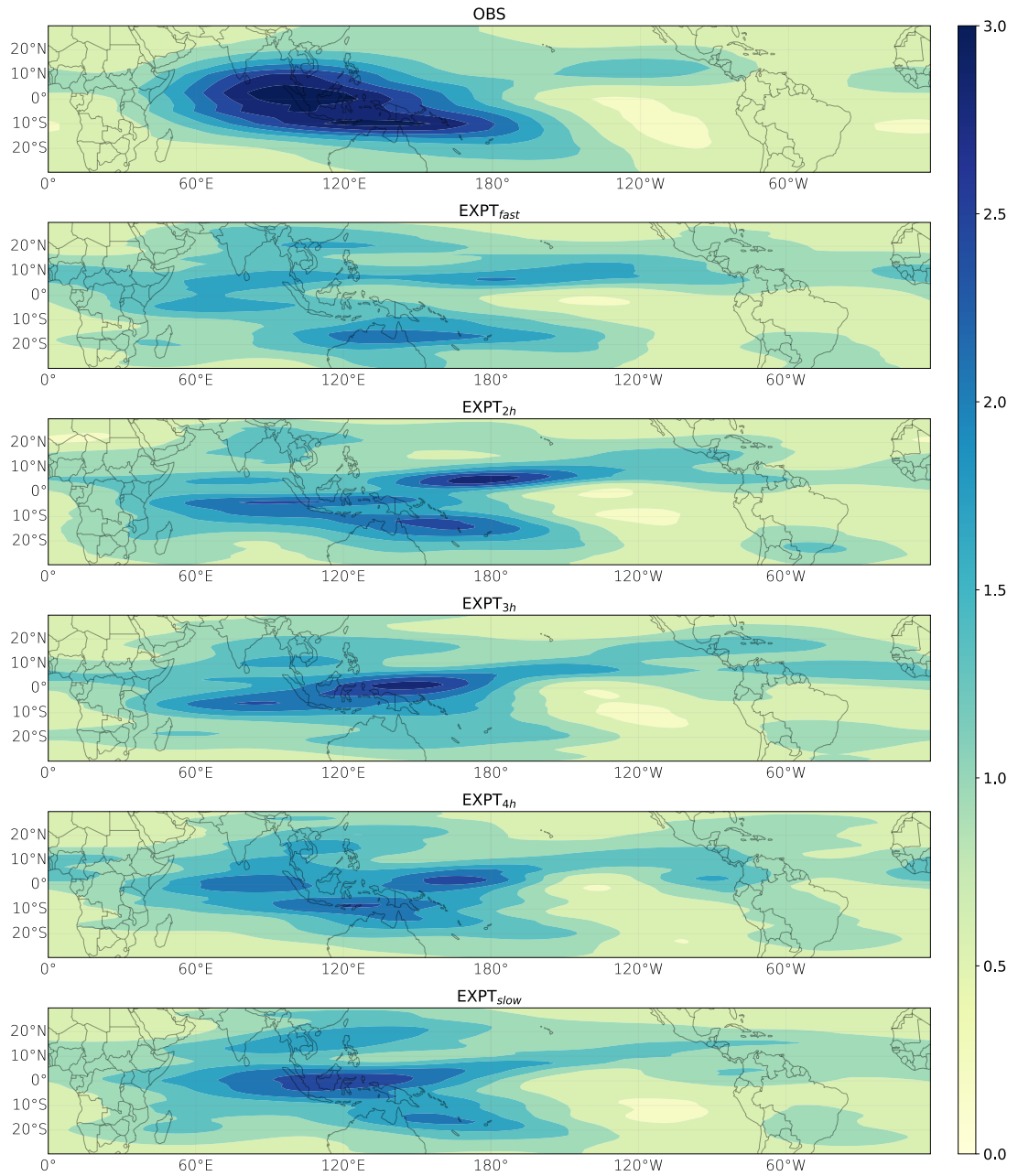


**Figure S4. MJO variance.** Same as Figure 6 of the main manuscript, except the variance fields are normalized by the respective domain means.